

PSB NASA

King

IN-47

028 580

FIRE Arctic Clouds Experiment

J.A. Curry¹, P.V. Hobbs², M. D. King³, D.A. Randall⁴, P. Minnis⁵

G.A. Isaac⁷, J.O. Pinto¹, T. Uttal⁶, A. Bucholtz⁸, D.G. Cripe⁴, H. Gerber⁹, C.W. Fairall⁶, T.J. Garrett²,
J. Hudson¹⁰, J.M. Intrieri⁶, C. Jakob¹¹, T. Jensen¹², P. Lawson¹², D. Marcotte⁷, L. Nguyen⁵,
P. Pilewskie¹², A. Rangno², D. Rodgers⁴, K.B. Strawbridge¹³, F.P.J. Valero⁸, A.G. Williams⁷, D. Wylie¹⁴

¹University of Colorado, Boulder

²University of Washington, Seattle

³NASA Goddard Space Flight Center, Greenbelt, MD

⁴Colorado State University, Fort Collins

⁵NASA Langley Research Center, Hampton, VA

⁶NOAA Environmental Technology Laboratory, Boulder, CO

⁷Atmospheric Environment Service, Downsview, Ontario, Canada

⁸Scripps Institute for Oceanography, La Jolla, CA

⁹Gerber Scientific, Inc., Reston, VA

¹⁰Desert Research Institute, Reno, NV

¹¹SPEC, Inc., Boulder, CO

¹²NASA Ames Research Center, Moffett Field, CA

¹³Centre for Atmospheric Research Experiments, Egbert, Ontario, Canada

¹⁴University of Wisconsin, Madison

Abstract

An overview is given of the FIRE (First ISCCP Regional Experiment) Arctic Clouds Experiment that was conducted in the Arctic during April through July, 1998. The principal goal of the field experiment was to gather the data needed to examine the impact of arctic clouds on the radiation exchange between the surface, atmosphere, and space, and to study how the surface influences the evolution of boundary layer clouds. The observations will be used to evaluate and improve climate model parameterizations of cloud and radiation processes, satellite remote sensing of cloud and surface characteristics, and understanding of cloud-radiation feedbacks in the Arctic. The experiment utilized four research aircraft that flew over surface-based observational sites in the Arctic Ocean and Barrow, Alaska. In this paper we describe the programmatic and science objectives of the project, the experimental design (including research platforms and instrumentation), conditions that were encountered during the field experiment, and some highlights of preliminary observations, modelling, and satellite remote sensing studies.

1. Introduction

The FIRE (First ISCCP (International Satellite Cloud Climatology Project) Regional Experiment¹) Arctic Clouds Experiment was conducted during April-July 1998 to study Arctic cloud systems under spring and summer conditions. The main goal of the experiment was to examine the effects of clouds on radiation exchange between the surface, atmosphere and space, and to study how the surface influences the evolution of boundary layer clouds. Observations collected during the field phase of the project will be used to evaluate and improve climate model parameterizations of Arctic cloud and radiation processes, satellite remote sensing of cloud and surface characteristics, and understanding of cloud-radiation feedbacks in the Arctic.

The strategy of the FIRE Arctic Clouds Experiment was to use research aircraft to obtain remote and *in situ* measurements of the properties of clouds and the sea ice/ocean surface. The NASA ER-2 flew at an altitude of 20 km with a suite of remote sensors that can be used to infer the characteristics of the surface and clouds below. Other aircraft, instrumented with *in situ* and remote sensing instruments, were used to measure radiation fluxes and the physical, optical and chemical properties of the clouds. The aircraft observations were made over surface-based observational sites in the Arctic Ocean and Barrow, Alaska.

FIRE's arctic field program interacted closely with the Surface Heat Budget of the Arctic Ocean (SHEBA) Project² (Moritz et al., 1993) and the Atmospheric Radiation Measurement (ARM)³ Program (Stokes and Schwartz, 1994). SHEBA, ARM and FIRE share scientific objectives that focus on improving simulations of arctic processes in global climate models and improving satellite retrievals of atmospheric state and sea ice conditions in the Arctic. SHEBA emphasizes the surface energy balance and the sea ice mass balance, while ARM is devoted to surface-based observations and modeling of clouds and radiation. The field component of SHEBA focused on an icebreaker ship deployed in the Arctic Ocean and left to drift for a year, which served as a floating science station. ARM provided a number of key surface-based radiometers and remote sensing

¹ FIRE is a U.S. national project that is funded primarily by the National Aeronautic and Space Administration (NASA); it includes participation of scientists from Canada, England, and Netherlands.

instruments designed to provide measurements of clouds and radiation at the SHEBA ice station. ARM also operates a duplicate set of instruments at Barrow as part of a decade-long program to monitor clouds and radiation on the north slope of Alaska.

The FIRE program, underway since 1983, is aimed at improving the simulation of clouds and radiation in large-scale models and enhancing satellite cloud retrieval techniques (Randall et al., 1995). FIRE Phase I (1984-1989) was designed to address fundamental questions concerning the characteristics of cirrus and marine stratocumulus cloud systems. FIRE Phase II (1989-1994) focused on more detailed questions concerning the formation, maintenance and dissipation of cirrus and marine stratocumulus cloud systems.

FIRE Phase III commences an investigation of arctic cloud systems. The FIRE Arctic Clouds Experiment, in collaboration with SHEBA and ARM, represents an important broadening of the scientific scope of the FIRE program. This strategic step was motivated by the importance of the Arctic for the global climate system, and an appreciation of how poorly we understand arctic clouds and the energy budget of the arctic surface. The purpose of this paper is to summarize the FIRE Arctic Clouds Experiment field operations and present some preliminary results. Section 2 presents a more thorough description of the project science objectives. Section 3 describes the research platforms and instrumentation. Section 4 provides an overview of the observations. Section 5 provides some preliminary highlights, including some comparisons of model results with the data.

2. Scientific Objectives

Motivated by the plans of SHEBA, FIRE and ARM to mount field experiments in the Arctic, Curry et al. (1996) prepared a review of research prior to 1995 related to arctic clouds and radiation; this review provides a background for the science objectives for the FIRE Arctic Clouds Experiment. Objectives relevant to large-scale numerical weather prediction and climate modeling in the Arctic are reviewed by Randall et al. (1998).

² SHEBA is a U.S. national program that is funded primarily by the National Science Program (NSF) and the Office of Naval Research (ONR); it includes international participation from Canada, Japan, and Russia.

³ ARM is sponsored by the U.S. Department of Energy (DOE).

The overarching objectives of the FIRE Arctic Clouds Experiment are to improve the satellite retrieval of cloud and surface characteristics in the Arctic, and to improve the representation of arctic clouds and radiation in general circulation models. Some background on these objectives is given below (following Curry et al., 1996), as well as specific science questions that have been formulated to address these issues.

2.1 *Clouds*

Observation of wintertime clouds in the Arctic are complicated by the presence of lower tropospheric ice crystal clouds, frequently referred to as “diamond dust,” which may increase surface downward longwave radiative fluxes by up to 40 W m^{-2} over those expected under clear-sky conditions. Some of these ice clouds may be produced by moist convective plumes associated with leads (openings in the sea ice) or may form as a result of the moistening of the boundary layer by a network of open leads. The ice clouds persist into the spring, perturbing solar radiation as well.

Summertime arctic stratus are often observed to form in multiple layers within a kilometer or so above the surface. In summer, a shallow, stably-stratified surface fog is often observed beneath a cloud-topped mixed layer. The upper cloud layers appear to form and persist without any turbulent mixing of moisture from the surface. On occasion, summertime boundary layer clouds have been observed to contain ice crystals.

During spring and autumn, boundary layer clouds are often mixed phase. Generally these seasons mark the transitions in the boundary layer from predominantly liquid boundary layer clouds of summer to predominantly crystalline clouds of winter. Aircraft data from previous field experiments reveal that ice may exist in clouds at temperatures as high as -4°C and supercooled liquid may occur at temperatures as low as -30°C .

Some key scientific issues relating to arctic clouds are:

- What is the influence of leads and other open water on cloud properties when large surface-air temperature differences exist?
- How does the extreme static stability and low atmospheric water vapor content of the lower troposphere, especially during winter, affect the flow of energy across the air-sea interface?

- What is the mechanism that leads to the spectacular multiple-layering of summertime cloud systems over the Arctic Ocean?
- How does the transition of low clouds from liquid to crystalline depend on temperature and aerosol characteristics, and how does the springtime transition differ from the autumnal transition?

2.2 *Radiation*

Clouds are the dominant atmospheric modulators of the arctic radiation climate. Cloud radiative properties depend on the amount of condensed water, the size and shape of the cloud particles, and the phase of the particles (liquid or ice). Recent studies of arctic clouds suggest that over the course of the year clouds have a net warming effect on the surface and that the top-of-the-atmosphere cloud radiative forcing is dominated by the shortwave flux.

The highly-reflecting snow/ice surface strongly affects the transfer of shortwave radiation. The surface albedo is influenced by meltpond area and depth, lead area, ice thickness and age, snow thickness and age, and overlying clouds. Clouds alter the spectral distribution of solar radiation and the relative amount of diffuse radiation. This has important consequences for the amount of radiation reflected by the surface, which depends on the spectral distribution and the ratio of direct-to-diffuse incoming solar radiation.

Because the central Arctic has little or no solar illumination during half the year, longwave radiation plays an especially important role in the radiation balance. The longwave opacity of the gaseous components of the arctic atmosphere is so low that clouds substantially increase the emission of longwave radiation both downward toward the surface and upward to space. Arctic stratus clouds often form in the warmest part of the lower troposphere, so that the downward longwave flux at the surface in winter can be larger than the upward flux from the sea ice. Simulation of longwave radiative transfer in the Arctic requires accurate modeling of water vapor absorption under the extremely cold and dry conditions that are typical of the polar regions.

Key scientific issues related to arctic radiation are:

- What is the spectral distribution of longwave radiation? In particular, what is the role of the 20 μm rotation-band “window” region in regulating the surface and atmospheric temperature in the Arctic?
- What are the effects of springtime “arctic haze” on the absorption of solar radiation in polar clouds?
- How do the transmittance and reflectance of solar radiation by clouds and the surface depend on the low solar zenith angles typical of the Arctic?
- What is the role of diamond dust in determining the radiation fluxes?
- What are the shortwave radiative effects of the horizontally inhomogeneous stratocumulus clouds over the inhomogeneous, highly-reflecting snow/ice surface?
- How do the optical properties of the arctic surface vary in response to changes in snow and ice characteristics (including melt ponds)?

2.3 *Aerosols*

The concentration and size distribution of cloud droplets depend in part on the aerosol in the atmosphere, specifically on the cloud condensation nuclei (CCN). CCN are quite variable in space and time, and this could lead to considerable variability in cloud microphysics, optical properties, and precipitation efficiency. CCN in the Arctic are composed primarily of sulfate, having both natural and anthropogenic sources. The interactions between clouds and aerosol are not simply one way; scavenging by clouds depletes CCN, but aerosol may also be produced and enhanced within the clouds through chemical and physical processes .

Ice particle concentrations in clouds may also be affected by aerosol, although this connection is more complex and less well understood. Sources of ice forming nuclei (IFN) include advected soil particles, air pollution, and oceanic biota. The concentration and composition of the IFN are hypothesized to be important for determining the phase of arctic clouds, and therefore their impact on the radiation balance.

In summary, key questions regarding the aerosols found in the arctic atmosphere are:

- What is the activity spectra of CCN and how does it vary?
- What are the sizes and composition of CCN, and how and why do they vary?

- How do the CCN distributions interact with the cloud droplet distributions?
- How do processes within arctic clouds modify CCN?
- What is the nature and source of IFN?
- Is it possible for ice particles to form at relative humidities below water saturation, via deposition nucleation?

2.4 Remote Sensing

Satellite retrievals of cloud and surface characteristics are hampered by: the complex vertical structure of the atmosphere, including temperature and humidity inversions; low temperatures and low water vapor amounts; little visible, thermal and microwave distinction between the clouds and the underlying surface; heterogeneity of the underlying surface; and the presence of complex cloud types (e.g., mixed phase clouds, thin multi-layered clouds).

Specific questions related to satellite remote sensing of arctic clouds include:

- How do the vertical variations of cloud and atmospheric properties affect the interpretation of satellite measurements of clouds?
- How well can surface and atmospheric radiative fluxes be reconstructed from satellite-based observations?
- What are the appropriate averaging periods for surface-based cloud observations so they can be meaningfully compared to satellite data? Do these averaging periods vary significantly as a function of cloud height and/or cloud type?
- How accurately can satellites detect the presence of clouds over ice and snow surfaces?
- What is the radiative significance of clouds that are not accurately detected by satellite?

3. Experimental design

The FIRE Arctic Clouds Experiment was designed to produce an integrated data set that:

- supports the analysis and interpretation of physical processes coupling clouds, radiation, chemistry, and the atmospheric boundary layer;
- provides *in situ* data for the testing of satellite and ground-based remote sensing analyses; and

- provides initial data, boundary conditions, forcing functions, and test data to support arctic modeling efforts.

The location and timing of the FIRE Arctic Clouds Experiment were determined by the scheduled operations of the SHEBA experimental site in the Beaufort Sea during October 1997 through October 1998. The Canadian Coastguard ice breaker *Des Groseilliers* was deployed in a multi-year ice floe on October 1, 1997, at 75°16.3' N, 142°41.2' W. The thickness of the undeformed multi-year ice at deployment was 1.7-2.0 m. Instrumentation was fully deployed and operational at the site by October 30. The ARM site at Barrow was fully operational by March 19, 1998, providing a secondary surface site for the experiment. Over the course of the field study, the SHEBA ice camp drifted considerably northwestward (Figure 1); it was at 78.5°N and 166°W by the end of July, 1998.

Four research aircraft were employed during FIRE (see Table 1). Flights were conducted in the immediate vicinity (50 km) of, and directly over, the SHEBA surface site and the ARM site at Barrow. The three medium-altitude aircraft made measurements spanning the period April 8 through July 30, 1998. In addition, during the period May 18 through June 6, the NASA ER-2 flew at an altitude of 20 km above either the University of Washington (UWa) Convair-580 or the NCAR C-130 aircraft. The timing of the aircraft missions, spanning the period from spring to mid summer, was designed to capture the transition between the wintertime boundary layer with predominantly ice clouds to the summertime boundary layer with predominantly liquid clouds, and to capture the onset of the sea ice melt season. This period was also selected as one for which both climate models and satellite remote sensing techniques are in particular need of improvements.

The flight plans of the three medium-altitude aircraft were designed to meet requirements for measuring both the horizontal variability and vertical structure of the atmosphere. Horizontal traverses of 20-200 km were made at various levels above, below and within cloud, in the boundary layer, and at various altitudes to map the surface using aircraft remote sensing instruments. Additionally, slow ascents and descents were made to obtain high-resolution vertical profiles using *in situ* instruments.

The timing of the flights was coordinated with satellite overpasses. The specific satellites of interest included:

- NOAA-12 and -14 Polar-orbiting Operational Environmental Satellites (POES). Aboard these satellites are the Advanced Very High Resolution Radiometer (AVHRR), which is a 4 or 5 channel radiometer measuring visible and infrared wavelengths, and the TIROS Operational Vertical Sounder (TOVS), which measures incoming radiation in the infrared and passive microwave with 27 channels.
- Defense Meteorological Satellite Program (DMSP) F12 and F13. Aboard this satellite are the SSM/I, which is a seven-channel, four frequency, linearly-polarized passive microwave radiometric system that measures brightness temperatures at 19.35, 22.235, 27, and 85.5 GHz; and the SSM/T2, which measures the brightness temperature near the 183.3 GHz water vapor line and also at 90 and 150 GHz.
- RADARSAT-1. Aboard this satellite is a Synthetic Aperture Radar (SAR), which sends pulsed microwave signals to Earth and processes the received reflected pulses.

The general strategy for FIRE's satellite remote sensing research is to use the aircraft primarily to evaluate remote sensing instruments at the surface and to extend the point observations made at the surface to the larger horizontal scale seen by satellites. The entire time series of surface-based remote sensing observations can then be used to evaluate and interpret satellite retrievals of cloud and surface characteristics. Coincident surface-based, aircraft and satellite measurements are essential for some validation exercises.

To meet the objectives of the FIRE Arctic Clouds Experiment, the following modeling activities are being undertaken:

- A variety of 1-D and 3-D radiative transfer models are being tested using near-instantaneous measurements of the radiation field and the atmospheric parameters that determine the radiation field (e.g., clouds, temperature, aerosol, trace gas concentrations).
- Large eddy simulation (LES) models are being used to develop parameterizations of cloud and boundary layer processes, which can eventually be incorporated into climate models.

- Improved parameterizations of physical processes for climate models are being tested against field observations using single-column models (SCMs). An SCM is a single vertical array of cells from a 3-D climate model, the forcing of which may be highly constrained so as to test individual parameterizations (Randall et al., 1996).
- To help in providing forecast guidance for the Canadian Convair-580 during this project, the Canadian Mesoscale Compressible Community Model (MC2) was run at 35 and 10 km resolution (Benoit et al., 1997).

The FIRE dataset must be readily accessible for modelers to use. To achieve this end, subsets of the data are being packaged so that they can serve as input files to models as well as for model validation. Specific integrated datasets that are being prepared (in collaboration with SHEBA and ARM) include: Integrated Radiative Flux dataset; Large-Eddy Simulation dataset; and Single-Column Model dataset.

3.1 Surface Observations

An extensive array of instrumentation was deployed at the SHEBA ice camp. Further information on the ship, its track, and instrumentation at SHEBA can be found on the SHEBA homepage (<http://sheba.apl.washington.edu>). Information regarding the instrumentation provided by the ARM program can be found on the ARM homepage (<http://www.arm.gov/docs/instruments.html>). The surface observations described below were of particular relevance to the FIRE Arctic Clouds Experiment.

Incident shortwave and longwave radiation fluxes were measured in detail by the ARM program, as well as by SHEBA and FIRE investigators. The following radiation instruments were deployed at the SHEBA ice camp:

- precision upwelling and downwelling infrared radiometers and shortwave spectral pyranometers;
- net radiometers;
- infrared thermometer (up- and down-looking; 9.6-11.5 μm);
- normal incidence pyheliometer (direct-beam solar irradiance; broadband);
- multi-filter rotating shadowband radiometer (0.415, 0.500, 0.665, 0.862, 0.940 μm ; spectral downwelling solar; direct and diffuse);

- multi-filter radiometer (upwelling solar; same wavelengths as rotating shadowband radiometer);
- Extended Range Atmospheric Emitted Radiance Interferometer (AERI) (absolute radiance from 4-20 μm with spectral resolution of 1 cm^{-1}); and
- Solar Spectral Flux Radiometer (SSFR) (solar irradiance spectrum from 0.30 - 2.2 μm with resolution of 5-15 nm, in both zenith and nadir directions).

These same instruments can be used to retrieve atmospheric temperature and humidity profiles, trace gases, aerosol characteristics, and cloud properties.

Cloud properties were measured from the SHEBA site, both remotely and using a tethered balloon. Remote measurements were made almost continuously for the duration of the SHEBA deployment. Instruments for remote measurements of cloud properties include:

- cloud radar (35 GHz; zenith up to 20 km height);
- micropulse lidar (0.5235 μm ; points in different directions up to 20 km height);
- microwave radiometer (23.8 and 31.8 GHz; integrated column water vapor and liquid amounts);
- ceilometer (0.905 μm ; detects cloud base height up to 7.5 km); and
- whole sky imager (cloud fraction).

To obtain *in situ* measurements of cloud properties, tethered balloons with instruments for cloud microphysical and radiation measurements were flown between March and June. Instruments flown on the balloons measured profiles in the lowest 1 km of the atmosphere of cloud particle concentrations and size distributions, and mean radiative intensities (actinic flux).

Meteorological data were obtained from:

- GPS rawinsondes (twice per day; four times per day during intensive observing periods);
- tethered balloon profiles of temperature, humidity and winds up to 1 km; and
- 10 m tower measurements of surface meteorology.

Properties of the near-surface atmospheric boundary layer were investigated using a 20 m tower. The tower was instrumented at several levels with:

- sonic anemometer/thermometer and fast-response hygrometer (eddy correlation measurements of turbulent fluxes);
- slow-response temperature, humidity, and wind sensors for measuring profiles.

Surface layer turbulence was also measured using a scintillometer system. This system propagates a 0.67 μm laser beam over a 400-m horizontal path 2-4 m above the surface, and thereby yields path-averaged values of the refractive index structure parameter and the turbulent fluxes of momentum and sensible heat.

SHEBA investigators conducted detailed measurements of the optical and physical characteristics of snow and sea ice, including snow depth, density and grain size, as well as ice temperature, salinity, density, brine volume and air volume. Studies were also conducted over lines ranging up to 20 km in length to assess the spatial variability of snow characteristics, surface albedo, and ice transmittance.

Observations of atmospheric state, cloud characteristics and radiation fluxes using nearly identical instruments to those at SHEBA were obtained at the ARM site in Barrow, Alaska, beginning March 19, 1998.

3.2 Aircraft Observations

Four research aircraft were deployed during the FIRE Arctic Clouds Experiment: the NASA ER-2, the National Center for Atmospheric Research (NCAR) C-130Q, the University of Washington (UWa) Convair-580, and the Canadian National Research Council Convair-580 (Table 1).

The NASA ER-2 is a single-engine, single-seat, high-altitude subsonic aircraft. The following instruments were deployed on the ER-2 during the FIRE Arctic Clouds Experiment:

- MODIS Airborne Simulator (MAS);
- Millimeter-wave Imaging Radiometer (MIR);
- Advanced Microwave Precipitation Radiometer (AMPR);
- Cloud Lidar System (CLS);
- High-resolution Interferometer Sounder (HIS);
- Solar Spectral Flux Radiometer (SSFR); and
- Airborne Multi-angle Imaging Spectroradiometer (AirMISR).

A summary of the instrument characteristics and derived data products are given in Table 2. Details of the instruments on the ER-2 can be found on the FIRE Arctic Clouds Experiment homepage (<http://eosweb.larc.nasa.gov/ACEDOCS/data/appen.d.2.html>).

The three medium-altitude aircraft shared some common instrumentation. In particular, many of the instruments to measure *in situ* cloud microphysical and aerosol characteristics were common to all three aircraft. Parameters measured by these aircraft include: aerosol concentration, composition and size distribution, cloud particle concentration and size distribution, liquid water content, droplet effective radius, particle shape, cloud condensation nuclei spectra, and ice nucleus concentration and composition. Specific cloud physics and aerosol instruments are listed in Table 3.

The NCAR C-130Q is a four-engine medium-altitude research aircraft that is designed to carry a payload of up to 13,000 lbs with full fuel load. The NCAR C-130Q measures atmospheric state parameters, turbulent fluxes, cloud physics, radiative fluxes, and also conducts remote sensing using scanning radiometers and video photography. In addition to the NCAR instruments, the C-130Q can support a large user-supplied payload. Some of the major research instrumentation deployed on the C-130Q for this experiment (excluding the cloud and aerosol instruments described in Table 3) included:

- Airborne Imaging Microwave Radiometer (AIMR) (Table 2);
- Multi-spectral Channel Radiometer (MCR) (Table 2); and
- Radiation Measurement System (RAMS), a multi-instrument array of radiometers consisting of: a Total Direct Diffuse Radiometer (TDDR; a shadowband radiometer with hemispheric field of view with 7 channels from near UV to the near IR); a Multichannel Radiometer (same as TDDR without shadowband; downlooking); up- and down-looking total solar broadband radiometers (0.2-3.9 μm); and up- and down-looking infrared broadband radiometers (4.125-48.25 μm).

The University of Washington (UWa) Convair-580 is a two-engine, medium-altitude research aircraft, which flew research missions for the first time in this experiment but deploying instrumentation that has been used frequently by the UWa on other aircraft. The UWa Convair-580 measures atmospheric state parameters, cloud physics, radiative fluxes, and aerosol chemistry. Some of the major research instrumentation deployed on the UWa Convair-580 for this experiment included:

- Aerosol optical properties: integrating nephelometer (aerosol backscatter coefficient); particle soot/absorption photometer (light absorption and graphitic carbon); scanning humidigraph

(humidification factor for aerosol light scattering).

- g-meter to measure optical scattering/extinction coefficients at 635 nm, asymmetry parameter, and back-to-forward scattering ratio for cloud and precipitation drops and ice particles.
- Cloud Absorption Radiometer (CAR): a scanning radiometer with 13 discrete wavelengths between 470 and 2300 nm; measures absorption and scattering of solar radiation by clouds and aerosols and bi-directional reflectance function.
- Solar Spectral Flux Radiometer (SSFR) (Table 2).

Measurements made by the g-meter represent the first time that the asymmetry parameter has been measured by aircraft.

The Canadian Convair-580 aircraft is nearly identical to the UWa Convair-580. The Canadian aircraft measured atmospheric state parameters, turbulent fluxes, cloud physics, radiative fluxes, and aerosol and air chemistry. Major research instrumentation deployed on the Canadian Convair-580 for this experiment included:

- Landsat simulator (Table 2);
- Radiometer (reflectance at 2 channels);
- Lidar (Table 2);
- Nephelometer (volume light scattering coefficient at 0.55 μm);
- IR pyrgeometer, SW pyranometer (broadband radiative fluxes; up- and down-looking);
- Concentrations of O_3 , SO_2 , and organohalogens;
- LiCor 6282 $\text{CO}_2/\text{H}_2\text{O}$ infrared gas analyzer, providing fast-response humidity and CO_2 measurements
- Aerosol chemistry: total organic carbon, speciated organics, inorganic and organic ions, black carbon, trace metals, and total organic carbon.

4. Overview of Experiment

The operational objectives of the FIRE Arctic Clouds Experiment were to make aircraft observations over the SHEBA ship during several months of spring and summer, using Fairbanks, Alaska, Barrow, Alaska, and Inuvik, Northwest Territories, as bases of operation. The logistics of

this experiment were quite complex. The SHEBA ship, initially deployed at 75.27°N, 142.69°W, was expected to drift to the westnorthwest about 320 nm by the end of the experiment (based upon buoy drift over the past 20 years). By the commencement of the Canadian Convair flights in April, the ship had moved to 76.12°N, 164.64°W, which was beyond the range of the Canadian Convair based in Inuvik. Hence, it was necessary for the Canadian Convair to refuel and overnight in Barrow when making flights to the SHEBA ship. During July, the ship was located in the vicinity of 78.11°N, 167.16°W, which required a one-way ferry of three hours for the C-130Q from Fairbanks, significantly diminishing flight time on station. The UWa Convair, based in Barrow, was in the best position to reach the SHEBA ship; nevertheless the SHEBA ship was 410 nm from Barrow by the end of its flights in June.

Logistical difficulties encountered at the SHEBA ship were often dramatic, but not unexpected based upon previous experience. Powerful storms during the first week of February and the second week of March caused significant production of ridges and open water at the surface, disconnecting or severing virtually all of the power cables to the instrumentation deployed on the ice. During the second week of March, the camp actually split into several floes that drifted in different directions, and a significant amount of equipment had to be moved so that all measurements were consolidated on a single flow. The early onset of snow melt at the end of May disabled the runway near the ship by mid June, necessitating arrangements for an icebreaker ship and helicopter for crew changeovers and the replenishment of supplies.

Communications from the ship to the mainland were handled by INMARSAT, which only advertises communication as far as 75°N. As the ship continued to drift northward, concerns were raised that the ship would lose satellite communication, but this did not happen. All four aircraft were able to communicate with the ship via high-frequency radio when they were within about 100 miles of the ship. This communication was extremely valuable in conducting the flights, since updates from the surface-based observations and satellite observations received on the ship via TERASCAN allowed modification of flight patterns to optimally sample the situation.

An additional consequence of the large westward drift of the SHEBA ship was that it left the Beaufort Sea (the original targeted region for the measurements) by the end of winter and moved into

the Chukchi Sea. The Beaufort Sea is characterized in summer and spring by a surface anticyclone and a predominance of stratus clouds. In the Chukchi Sea, the weather situation was more dynamic with southerly flow predominating during June and July, bringing in high clouds that were often associated with frontal systems. Because the SHEBA ship was often on the edge of the anticyclone or affected by small storms, forecasting the weather for flight operations was difficult, particularly during July, with conditions often changing rapidly. The difficulty in forecasting the weather, combined with the long ferry flight to the SHEBA ship, made it difficult to make flight plans before actually receiving radio communication from the ship about an hour before arriving at the site.

Table 4 gives an overview of the conditions sampled by the three medium-altitude research aircraft during the FIRE Arctic Clouds Experiment. A variety of conditions were sampled, including clear skies, boundary layer clouds, mid- and upper-level clouds, and clouds in the presence of open leads. Various flight patterns were flown, aimed at evaluating surface-based, satellite, and ER-2 remote sensing instruments, and providing input for evaluating and modeling cloud-radiative interactions, boundary layer clouds, surface albedo and radiation fluxes,

During the period of aircraft measurements (April through July, 1998), cloud and surface conditions over the ice changed from near-winter conditions with boundary-layer ice clouds and a snow-covered surface, to the peak of the summer melt season with abundant melt ponds and liquid clouds in the boundary layer. An overview is given below of the weather, cloud and surface characteristics at the SHEBA ship for each of these four months.

April. At the beginning of the Canadian Convair-580 flights on April 8, the surface air temperature at SHEBA was -13°C ; at the end of the flights on April 29 the temperature was -18°C . During mid-April there was a 4-day period when the surface air temperature remained unseasonably warm, above -10°C . Boundary layer clouds sampled in the vicinity of the ship were entirely liquid on April 17, when cloud temperatures were -5 to -10°C , and entirely crystalline on April 21 when cloud temperatures were -15 to -20°C . The synoptic situation in April was dominated by a surface high northeast of the ship with a broad weak cyclone in the lower Chukchi Sea and along the Alaskan coast. This combination produced easterly surface winds most of the time with southerly or southeasterly winds aloft. Deviations occurred when a cyclone moved north out of the Bering

Straight, crossing the SHEBA ship on 18-21 April, and a surface anticyclone invaded from the northwest during 24-26 April. Some of the Canadian flights took place close to the coast between Inuvik and Barrow, and included sampling open water regions associated with leads and polynyas.

May. During May, 1998, the C-130Q, ER-2, and UWa aircraft conducted research flights. May was dominated by an anticyclone to the east of the ship which moved north later in the month. A persistent cloud-topped surface mixed layer was present from April 30-May 19. Surface-based mixed layers are thought to be rare in Arctic, although they are most likely to occur during May when the surface warms rapidly. At the SHEBA ship steady warming at the surface was evident, with temperatures of -20°C at the beginning of the month and 0 to -2°C at the end of the month. Early in the month, two leads opened in the vicinity of the SHEBA ship, several hundred meters wide. These leads froze and re-opened intermittently during the month, but during the latter half of the month there was virtually no open water in the vicinity of the SHEBA ship. At the end of the month, snow melt began, which was accelerated by several days of rain.

June. June weather was characterized by an anticyclone east of the SHEBA ship, which moved into Canada on occasions. The ship was generally under a southerly flow caused by weak cyclones and upper air troughs to the west. During the first week of June, there was a near balance between upwelling and downwelling longwave radiation at the surface; however, the net shortwave radiation of about 150 W m^{-2} near solar noon contributed significantly to snow melt and the development of melt ponds. Clouds were clearly warming the surface; during clear sky periods the net radiation became negative and the surface changes from melting to freezing. The surface melting was somewhat sporadic, interrupted by periods of surface freezing induced by clear skies and/or high surface winds. By the third week in June, most of the snow had melted. During June, multi-layered clouds were most commonly encountered, with the bases and tops of a given layer varying appreciably over relatively short distances.

July. July was a fairly stormy month, with persistent southerly flow from the North Pacific Ocean and frequent mid- and high-level clouds. A strong surface temperature inversion characterized the region from July 17 to 30, the strength of the surface inversion reaching as high as 12°C . Periodically, a shallow surface-based mixed layer less than 100 m deep would develop under conditions of high wind speeds or a surface fog, especially during the first half of the month.

Boundary-layer clouds were entirely liquid in phase. Surface characteristics evolved over the course of the month, with increased melt pond coverage and open water, and corresponding decreases in surface albedo.

5. Some highlights of preliminary results

In this section we present selected examples illustrating the technology used in the experiment and how the dataset can be synthesized and integrated to help improve modeling and satellite remote sensing and to address key scientific questions.

5.1. Clouds

Among the numerous cloud situations observed during the experiment, we describe here two cases that illustrate some data and some preliminary findings on cloud particle phase.

Measurements of cloud characteristics are illustrated for May 4 using C-130Q and surface-based observations. The time series of cloud radar returns (see Fig 2) shows a persistent boundary layer cloud (-15 dBz) surmounted by sporadic altostratus clouds (-40 dBz) that had almost disappeared by 22 UTC when the C-130Q arrived on site. The boundary layer is characterized by a cloud-topped mixed layer (Figure 3), with cloud top at 1080 m and base at 660 m. The humidity inversion above the cloud-topped mixed layer appears to have contributed to the homogeneity and persistence of the cloud deck. Such humidity inversions are rare outside the polar regions; they are hypothesized to be associated with moisture advection and precipitation drying of the lower atmosphere (by diamond dust, snowfall and drizzle). Profiles of liquid and ice water content (Figure 3c) shows that the cloud was mixed phase, with slightly more than half of the condensed water in the crystalline phase. This is consistent with the lidar depolarization values in Fig 2b, where depolarization values less than 0.2 indicate the presence of liquid water between 660 and 1100 m. The ice water content in Figure 3b was determined from the Cloud Particle Imager (CPI), using images such as those shown in Figure 4. Also determined from the CPI are size spectra of the ice particles (Figure 4). CPI images taken above the cloud show rosettes $> 500 \mu\text{m}$, columns with side plane growth and small ice particles; presumably these particles have fallen from the dissipating altostratus cloud. These large particles

accreted drops as they fell through the mixed-phase cloud and likely account for the presence of relatively large (up to 1 mm) rimed ice particles in this shallow cloud. The regions with large rimed particles also account for the peaks of up to 0.4 g m^{-3} in the ice water content (Figure 3c). Below cloud, precipitation in the form of mostly rimed ice particles was observed. Near the SHEBA ship, ice forming nucleus (IFN) concentrations were quite small, $< 0.5 \text{ liter}^{-1}$ at -22°C at a water supersaturation of 3%. Above cloud top the IFN concentration was $\sim 25 \text{ liter}^{-1}$ at -27°C . Condensation nuclei (CN) at low levels were fairly uniform ($\sim 200 \text{ cm}^{-3}$), indicating relatively clean air.

One of the unusual cloud types that occurs over sea ice during the cold portion of the year is convective clouds emanating from open water in leads or polynyas. Figure 5 depicts a low-level transect by the Canadian Convair 580 aircraft across Cape Bathurst Polynya in the Beaufort Sea (near 70°N , 135°W) on April 25, 1998. The lowest panel shows output from a downward-looking multispectral Landsat spectrometer in the wavelength interval $0.45\text{-}0.52 \mu\text{m}$ with a 15° field of view. Clearly evident is the sharp transition from solid sea ice to open water on the southern edge of the polynya (point A), with thin ice and leads (between points B and C) characterizing the region to the north of the polynya. The upper two panels show ambient temperatures and humidities along the transect and eddy correlation fluxes of the same quantities. Advection of cold air over the relatively warm open water resulted in positive sensible heat and moisture fluxes between points A and B, leading to potential temperatures and specific humidities increasing in the downwind direction across the polynya. The sensible and latent heat fluxes resulted in the formation of a shallow convective cloud over the polynya that is advected downwind (Figure 6) on 27 April.

Large variations in the relationship between cloud temperature and phase of the arctic clouds were seen in this experiment, consistent with previous observations (e.g., Curry et al., 1996; Hobbs and Rangno, 1998). During May, liquid water was observed by the C-130Q in mixed phase clouds at temperatures as low as -23°C , while during June the UWa Convair-580 observed ice crystals in mixed phase clouds at temperatures as high as -4°C . In the absence of ice particles falling from above such as was the case in Figure 4, the occurrence of ice in the boundary layer clouds appears to be related to maximum droplet sizes. For example, ice crystals were present between -4 and -6°C when the cloud droplets were large ($> 25 \mu\text{m}$ diameter, also typically some drizzle drops present) and in

concentrations of at least a few per cm^3 . Overall cloud droplet concentrations were low ($<100 \text{ cm}^{-3}$) in these cases as well. Conversely, colder boundary layer clouds (down to around -12°C) with smaller cloud droplets generally did not contain ice. Also, overall cloud droplet concentrations were higher ($>100 \text{ cm}^{-3}$) in these cases. These observations support the picture presented by Hobbs and Rangno (1998).

5.2 Aerosols

During the FIRE Arctic Clouds Experiment, the atmosphere was frequently pristine near the surface. However, haze layers several hundreds to thousands of meters thick were common aloft, indicating long-range transport. Figure 7 shows an example of a vertical profile flown through a thick haze layer that probably originated in Asia. Tenuous cirrostratus cloud was present above 5 km; at 100 m altitude there was a very thin (16 m) stratus layer. The profiles shown in Fig. 7 show relatively high values of extinction and scattering at altitudes exceeding 4000 m, and the haze layer shows considerable structure. The extinction coefficient has at least eight distinct maxima over the depth of the profile. Furthermore, within each maximum there are varying degrees of absorption, suggesting differing sources and/or aging of the aerosol.

Within 100 m of the surface, Figure 7 shows that extinction and scattering were very low. Accumulation-mode particle concentrations were ten times greater aloft than at the surface. Precipitation scavenging of these particles by boundary-layer stratus may have created these unusually clean conditions near the surface. During May, the C-130Q generally observed very low concentrations of CN (condensation nuclei), CCN (cloud condensation nuclei) and IFN (ice forming nuclei) in the boundary layer, indicating a very clean background and fairly efficient or long duration scavenging mechanisms. CN values of $\sim 10 \text{ cm}^{-3}$ for extended periods are among the cleanest in the world. Occasionally during May, the NCAR C-130Q observed small-scale regions near the surface with high concentrations of aerosol particles, particularly IFN, possibly associated with open water in leads. It has been hypothesized that ocean bacteria may be active as ice nuclei, but it is not clear how these could enter into the atmosphere from the small areas of open water in the Arctic Ocean.

During July, very high concentrations of small aerosol particles were observed from the C-130Q in the boundary layer. Volatility tests suggest that the particles are sulfuric acid, which is

consistent with local production of dimethyl sulfide (DMS) in the Arctic Ocean (Ferek et al., 1995). Local production of aerosols was also observed in the humidity inversion above boundary layer clouds and also in dissipating cloud layers. In about 30% of the cloudy boundary layer cases sampled by the UWa Convair-580, the total particle concentrations in a layer just above the top of the cloud layer were $\sim 1,000 \text{ cm}^{-3}$ (in some cases $\sim 8,000 \text{ cm}^{-3}$) greater than those immediately above or below the layer. The cases with enhanced particle concentrations above cloud top were associated with a cloud top temperature and a humidity inversion (e.g. see Figure 3). It appears that nucleation-mode particles were probably responsible for the increases in total particle concentrations, possibly having formed by gas-to-particle conversion in the layer of enhanced humidity. A similar phenomena was observed from the C-130Q. In some cloud layers, even after the clouds had dissipated, enhanced CN (but not IFN) were observed, presumably associated with particle production by gas-to-particle conversion in the humid air.

On 14 June, between 1950 and 2130 UTC, the UWa Convair-580 aircraft flew a series of three horizontal transects through the lower, middle and upper portions of a uniform stratus cloud about 200 m thick. The transects were flown from 43 km downwind of Barrow (point A) to 129 km downwind of Barrow (point B). Transects flown below the cloud and in the cloud showed a clear gradient in interstitial CN concentrations, with concentrations highest closest to Barrow. These measurements point to the advection and dispersion of an anthropogenic plume downwind of Barrow. The effects of particle emissions from Barrow on the microstructure of the stratus cloud was readily apparent. Mean droplet concentrations in the vicinity of A and B were 68 cm^{-3} and 25 cm^{-3} , respectively. The mean values of the cloud droplet effective radius at A and B were $9.5 \mu\text{m}$ and $11.1 \mu\text{m}$, the mean drizzle fluxes at A and B were 0 and 1.7 mm day^{-1} , and the mean liquid water contents at A and B were 0.18 and 0.15 g m^{-3} . Thus, the Barrow plume increased droplet concentrations in the stratus, decreased droplet effective radius, and effectively shut off drizzle. These observations highlight the sensitivity of arctic stratus clouds to modification by anthropogenic aerosol.

5.3 Radiation

Numerous radiometers on the aircraft and at the surface provide a detailed picture of the radiation environment in the vicinity of the SHEBA ship. Here we describe some elements of the surface and cloud radiation characteristics.

The evolution of area-averaged surface albedo (obtained from the ratio of the upwelling to downwelling broadband solar flux) in the vicinity of the SHEBA ship, measured by the UWa Convair-580 and the NCAR C-130Q, is shown in Fig. 8. During May, the average surface albedo values for the six NCAR C-130Q flights where the surface could be observed ranged from 0.85 to 0.67. There was no obvious change in amount of open water and new ice. The highest albedo (0.85) was measured on May 18 after a fresh snowfall beneath an optically thick liquid cloud. The lowest value of 0.67 was measured under a clear sky on May 20. On May 29, the first rainfall of the season caused melt metamorphism to begin and the first surface melt ponds began forming during the first week of June. The largest gradient in surface albedo occurred during the period June 7-18, when most of the snow melt occurred. By June 18, most of the surface snow had disappeared. Area-average surface albedos in the vicinity of the ship ranged from 0.42 to 0.56 during July, depending on the evolution of the surface melt and the cloud characteristics. Surface albedo was strongly influenced by cloud optical depth. On July 18, we determined a totally diffuse surface albedo of 0.56 in the vicinity of the ship under heavy overcast. Just east of the ship under clear sky conditions, with no obvious differences in surface features, the surface albedo was 0.40.

During April and the first half of May, considerable inhomogeneities in upwelling radiation were seen, associated with ice of different thickness and also open water. Figure 9 shows a time series of hemispheric upwelling shortwave and longwave radiation obtained on 7 May from the C-130 at an altitude of 30 m. Surface temperatures ranged from -15°C over multi-year ice to -1.7°C over open water. The impact of leads on the upwelling fluxes is seen in Figure 9 from the coincident low values of upwelling shortwave radiation and the high values of the upwelling longwave radiation. During July, when the sea ice was melting, the surface was very complex (see cover), with open water in leads and the surface melt ponds clearly influencing the surface albedo (the hemispheric shortwave radiometers were not capable of resolving the individual small features).

The NASA Ames Solar Spectral Flux Radiometer (SSFR) was deployed on the NASA ER-2, on the University of Washington CV-580, and on the SHEBA ship. Figure 10 shows 22 consecutive hours of spectra of spectral downwelling irradiance at the SHEBA ship on 15-16 May. Local noon is around 23 UTC and coincides with maximum signal in clear sky on 15 May; the minimum solar elevation is 6° at approximately 11 UTC. Before 03 UTC, water vapor and oxygen features dominate the spectra. By 04 UTC the effects of cloud are clearly seen by the saturated oxygen band at 762 nm and water vapor band at 940 nm.

Measurements of the diffuse radiation field reflected by arctic stratus clouds and sea ice were measured aboard the UWa Convair-580 aircraft while flying a clockwise circular orbit and scanning the scene below the aircraft with the NASA-Goddard scanning radiometer (CAR). This radiometer scans at a rate of 100 rpm from zenith to nadir on the starboard side of the aircraft and can map the entire reflection pattern of the surface during a complete circular orbit of the UWa Convair-580. With a 1° field of view of the radiometer, a complete bidirectional reflectance distribution function (BRDF) can be obtained for eight wavelengths of the radiometer simultaneously (King, 1992). Figure 11 shows the reflectance function at 0.68 and 1.64 μm for a homogeneous stratus cloud and for the sea ice surface. Of particular interest in Figure 11a is the enhanced backscattering maximum for the stratus cloud that occurs in opposition to the sun. Surrounding this glory feature was a pronounced rainbow (apparent on the left-hand side of Fig. 11a, which is characteristic of water droplet clouds). Figure 12b illustrates the reflection function of sea ice. In contrast to Fig. 11a, sea ice shows no rainbow or glory pattern, and is considerably darker than stratus water clouds at 1.64 μm due to the much larger absorption of solar radiation by ice than water at this wavelength.

5.4 Remote Sensing

Remote sensing data from the NASA ER-2 are illustrated in Figure 12 for a case on May 20 near the coast of Barrow. The swath includes tundra covered by snow (and cloud), open water near the coast, and sea ice floes off shore. The ER-2 was flying down the image from top to bottom, encountering single layer stratus clouds with a cloud top altitude of around 600 m (CLS). Clouds are readily observed by the MAS at 1.62 μm since water clouds are quite reflective at this wavelength, in contrast to open water and sea ice which are both quite dark at this wavelength. The MAS visible

image ($0.66\ \mu\text{m}$) suggests that the clouds are optically thick over the tundra, thinning and becoming semi-transparent over the open water. This is also confirmed by examining the vertical cross-section of the CLS. The AMPR 37 GHz image clearly shows the surface features, since atmospheric emission at this wavelength is minimal. Open water has low emissivity and hence low brightness temperature at the AMPR frequency of 37 GHz, while snow and ice have high emissivity at 37 GHz and hence appear bright. Comparison of the images at 220 and 37 GHz (MIR) shows that over open water the brightness temperature at 220 GHz is significantly higher because of the higher surface emissivity and significant atmospheric emission at this frequency. Over sea ice, the low brightness temperature at 220 GHz (but not at 37 GHz) indicates that there is some snow cover on the sea ice, which the 220 GHz sees because of its shallower penetration depth. This case illustrates the complexity of the polar surfaces and utility of the combination of visible, near infrared, submillimeter, and microwave wavelengths in separating out the characteristics of the surface and clouds.

An example of a retrieval of cloud properties from the NOAA-14 AVHRR is shown in Fig. 13 for 2300 UTC, 4 May 1998 (corresponding to the case described in Figures 2-4). The satellite data consist of 1 km AVHRR data taken over the SHEBA Ice Station ($76.0^\circ\ \text{N}\ 165.4^\circ\ \text{W}$). Figure 13a shows the channel 3 ($3.75\ \mu\text{m}$) image that depicts a relatively complex cloud system over the area. The data taken in the box centered over the SHEBA ship (outlined in the satellite image) were analyzed with the solar-infrared, infrared, split-window technique (SIST) that matches calculations from radiative transfer parameterizations of reflectance and emittance at 3.75 , 10.8 , and $11.9\ \mu\text{m}$ to determine cloud phase, particle size, and optical depth for each pixel (Minnis et al., 1998). Of the 870 pixels, 18% were classified as liquid water and 82% as ice. The mean effective radius for the water droplets was $6.3\ \mu\text{m}$, while the mean effective diameter for the ice crystals was $10.2\ \mu\text{m}$. Images of the retrieved particle sizes and optical depths are shown in Figure 13e. The C-130 *in situ* instruments observed high concentrations of small, nearly spherical particles near cloud top. Further into the cloud, some liquid water was observed with indications of icing and some drizzle. These observations provide tentative confirmation of the satellite retrievals of cloud particle size and phase. The radar and flight logs, however, show that the retrieved altitude is overestimated by almost 3 km.

During July 1998 the NOAA-15 AVHRR became available. This instrument differs from previous AVHRRs because the channel 3 measures 1.6 μm radiances during the daylight and 3.75 μm radiances at night. NOAA-15 is the first operational meteorological satellite with the 1.6 μm channel. This spectral band provides extremely good discrimination of snow, clouds, ocean, and land as shown in the multispectral image in Fig. 14. It is also useful for cloud phase and particle size determination. Snow crystals and water bodies are strong absorbers so that they appear black in the 1.6 μm imagery. Land surfaces are typically more reflective at 1.6 μm than at 0.63- μm while ice clouds are less reflective than liquid clouds. Thus, the combination of the visible, infrared, and 1.6- μm images shows the cold ice pack as pink, clouds as white and the clear water as deep blue. Thin clouds over the ice indiscernible in either visible or infrared images are quite evident in the 1.6 μm image and multichannel overlay. The new AVHRR data should provide much improved satellite retrievals of cloud properties over Arctic. The aircraft flights during July 1998 should be very valuable for validating the interpretation of this new satellite resource.

5.5 Single-Column Modeling

Data obtained during the FIRE Arctic Clouds Experiment has been used to assess the performance of several large-scale models during May: the European Centre for Medium Range Weather Forecasting (ECMWF) numerical weather prediction model as it was operational at the time of the experiment, and single-column versions of the Colorado State University (CSU) (Fowler et al., 1996) and the Arctic Regional Climate System Model (ARCSyM) (Pinto et al., 1998). The single-column models are forced with time series of large-scale advective tendencies and divergences obtained from the ECMWF initialized analyses. The surface turbulent fluxes were specified using ECMWF data in the CSU SCM, while turbulent fluxes were modeled in the ARCSyM SCM. The ECMWF column is not allowed to develop its own short-term climate since results are from successive global 12-36 hour forecasts; therefore, the simulation is not susceptible to model drift as are the two SCMs described above.

Table 5 shows a comparison of the monthly-averaged values for May of selected cloud and radiation parameters for the ECMWF, CSU, and ARCSyM models against the field observations. The surface radiation fluxes were obtained from the tower near the SHEBA ship; cloud fraction, base and top heights were determined from the cloud radar and lidar; and cloud liquid water path (LWP) was

obtained from both the surface-based microwave radiometer and aircraft *in situ* measurements made by the C-130Q aircraft. None of the observations are in their final state at this time.

The ECMWF and ARCSyM models underpredict the total cloud fraction. Cloud fraction estimates obtained individually from the lidar and radar differ by a few percent, but this discrepancy is small relative to the discrepancy with the model simulations. A substantial portion of the underestimation of cloud fraction by the models arises from underprediction of low clouds, indicated both by the low cloud fraction and the base of the lowest cloud layer. The ECMWF model is fairly successful at reproducing the observed cloud heights. Although the CSU modeled total cloud fraction agrees well with the observations, the model appears to be producing more high clouds and fewer low clouds than was observed. All three models substantially underpredict the LWP.

All three models predict surface net shortwave radiation fluxes that are too large and surface downwelling longwave radiation fluxes that are too small. The modeled surface radiation fluxes are consistent with model underprediction of cloud fraction and liquid water path. The modeled net solar flux has two types of errors in the ARCSyM. The modeled net solar flux is too large when clouds are present but not optically thick enough in the model. The modeled net solar flux is too small during clear sky periods, indicating that either the clear sky albedo or the clear sky attenuation is too large. In the CSU SCM the net solar flux at the surface shows a clear bias, overpredicting the amount of solar radiation absorbed by the surface. The ECMWF model does fairly well at simulating clear-sky longwave fluxes but tends to underestimate the DLWR during cloudy periods. In the shortwave the ECMWF has a bias similar to that seen in the CSU SCM.

Further details of the intercomparison of the observations with the SCMs are shown in Figure 18 for the time series of cloud liquid water path (LWP) and surface radiation fluxes. The LWP values were obtained during vertical profiling through cloud layers by the C-130Q research aircraft by the surface microwave radiometer. The models tend generally to underpredict the LWP, with liquid clouds more persistent in the CSU SCM. Both models have LWP values less than 30 g m^{-2} during the first 3.5 weeks of May, while observed values are as large as 120 g m^{-2} during the same period. Reanalysis of the microwave and aircraft datasets may bring the observed and simulated values closer, but it appears that there is a consistent underprediction of LWP by all three models. The modeled downwelling longwave radiation is simulated fairly well in the ARCSyM SCM during clear sky periods,

while the CSU SCM underestimates the clear sky fluxes by over 50 W m^{-2} . During periods when the occurrence of liquid clouds are accurately modeled, the modeled downwelling longwave radiation is simulated fairly well. Major discrepancies between the modeled and observed downwelling longwave radiation may be related to missing the occurrence of a cloud event or inaccurately representing cloud layers as crystalline (i.e., not optically thick enough). This occurs in the CSU SCM on 9-12 May and in the ARCSyM SCM on 12-15 May.

6. Conclusions

The FIRE Arctic Clouds Experiment successfully met its operational objectives: to conduct a multi-aircraft study over the Arctic Ocean in the vicinity of the SHEBA ice station and the ARM Barrow site. Preliminary analysis of the data indicates that the dataset will provide a wealth of information on clouds, radiation, and aerosol to address the science, remote sensing, and modeling objectives of the project.

Ultimate achievement of the full objectives of the FIRE Arctic Clouds Experiment will require extensive analysis of the data and comparison with models and satellite retrievals by a large number of scientists, both within and beyond the FIRE Science Team. To facilitate collaboration, the datasets are being archived in a form that will make them readily accessible worldwide. Further information on the FIRE Arctic Clouds Experiment and data archival can be found at (http://eosweb.larc.nasa.gov/ACEDOCS/ace_intro.html and <http://ltpwww.gsfc.nasa.gov?MAS/FIREIII.pdf>).

Acknowledgements. The FIRE Arctic Clouds Experiment was funded by National Aeronautics and Space Administration, National Science Foundation, Department of Energy, Environment Canada, the Canadian National Research Council, and the Canadian Panel on Energy Research and Development. We would like to acknowledge the following individuals and groups that assisted during the field experiment: D. McDougal and the FIRE Project Office, K. Laursen and the staff of the NCAR Research Aviation Facility, the flight crews of the UWa and Canadian Convair-580s, the U.S.

Army at Fort Wainwright, the Geophysical Institute at the University of Alaska, the NASA Langley DAAC and Research Center Communications and Computer Systems Branch, scientists and technical personnel on the *Des Groseilliers*, and all of the scientists, students, and technical personnel that participated in the field experiment. We are grateful to the ECMWF for providing a special assimilated dataset for the single-column model experiments. We would like to also thank R. Hood, J. Wang, J. Spinhirne, the ARM program, and the SHEBA Project Office for contributing data to this paper. Members of the FIRE Arctic Science Team are C. Bretherton, W. Cotton, J. Curry, A. Del Genio, W. Eberhard, C. Fairall, H. Gerber, J. Hallett, C. Jakob, P. Hobbs, J. Hudson, G. Isaac, M. King, Y. Kogan, S. Kreidenweis, S. Krueger, P. Lawson, D. Lenschow, M. Miller, P. Minnis, P. Pilewskie, D. Randall, B. Rossow, J. Spinhirne, S. Tsay, T. Uttal, F. Valero, S. Wang, Q. Wang, B. Wielicki, D. Wylie.

References

- Benoit, R., M. Desgagne, P. Pellerin, Y. Chartier, and S. Desjardins, 1997: The Canadian MC2: a semi-lagrangian semi-implicit wideband atmospheric model suited for finescale process studies and simulation. *Mon Wea. Rev.*, 125, 2382-2415.
- Curry, J.A., W.B. Rossow, D. Randall and J.L. Schramm, 1996: Overview of Arctic cloud and radiation properties. *J. Clim.*, 9, 1731-1764.
- Ferek, R.J., P.V. Hobbs, L.F. Radke, J.A. Heering, W.T. Sturges, and G. F. Cota, 1995: Dimethyl sulfide in the arctic atmosphere. *J. Geophys. Res.*, 100, 26093-26104.
- Fowler, L. D., D. A. Randall, and S. A. Rutledge, 1996: Liquid and Ice Cloud Microphysics in the CSU General Circulation Model. Part I: Model Description and Simulated Microphysical Processes. *J. Climate*, 9, 489-529.
- Hobbs, P. V., and A. L. Rangno, 1998: Microstructures of low- and middle-level clouds over the Beaufort Sea. *Q. J. Roy. Meteor. Soc.*, 124, in press.
- King, M. D. (1992). Directional and spectral reflectance of the Kuwait oil-fire smoke. *J. Geophys. Res.*, 97, 14545-14549.
- Minnis, P., D. P. Garber, D., F. Young, R. F. Arduini, and Y. Takano, 1998: Parameterization of reflectance and effective emittance for satellite remote sensing of cloud properties. *J. Atmos. Sci.*, 55, 3313-3339.
- Moritz, R.E., J.A. Curry, N. Untersteiner, and A.S. Thorndike, 1993: *Prospectus: Surface Heat Budget of the Arctic Ocean*. NSF-ARCSS OAI Tech. Rep. 3, 33 pp.
- Pinto, J.O., J.A. Curry and A.H. Lynch, 1998: Modeling clouds and radiation for the November 1997 period of SHEBA using a column climate model, *J. Geophys. Res.*, in press.
- Randall, D.A., B.A. Albrecht, S.K. Cox, P. Minnis, W. Rossow, and D. Starr, 1995: On FIRE at ten. *Adv. Geophys.*, 38, 37-177.
- Randall, D.A., K.-M. Xu, R.J.C. Somerville and S. Iacobellis, 1996: Single-column models and cloud ensemble models as links between observations and climate models. *J. Clim.*, 9, 1683-1697.
- Randall, D.A., J.A. Curry et al., 1998: Status of and outlook for large-scale modeling of atmosphere-ice-ocean interactions in the Arctic, *Bull. Am. Meteorol. Soc.* 79), 197-219.
- Stokes, G. M.; Schwartz, S. E., 1994: The Atmospheric Radiation Measurement (ARM) Program: programmatic background and design of the cloud and radiation test bed, *Bull. Amer. Meteorol. Soc.*, 75, 1201-1221.

Table 1 - Overview of aircraft platforms

Aircraft	Altitude (ft)	Base	Flight Period (1998)	# of flights over SHEBA	# of flights over Barrow
NASA ER-2	60,000	Fairbanks	5/18 - 6/6	8	11
NCAR C-130Q	100-25,000	Fairbanks	5/4 - 5/27 7/8 - 7/30	8 8	0 0
UWa Convair-580	50-32,000	Barrow	5/19 - 6/24	8	11
Canadian Convair-580	50-25,000	Inuvik	4/8 - 4/29	4	2

Table 2. Airborne remote sensing instrumentation. Swath width and pixel size are determined for typical aircraft flight levels (20 km for the ER-2; 4 km for the NCAR C-130).

Sensor	Wavelengths	Scanning Mode	Swath Width	Pixel Size	Data Products
ER-2					
MAS	0.47-14.3 μm 50 bands	cross track	86 km	50 m	solar spectral radiance bidirectional reflectance cloud particle phase and size, optical depth
MIR	89, 150, 183.3 \pm 1 183.3 \pm 3, 183.3 \pm 7 220, 340 GHz	cross track	42 km	1 km	surface emissivities cloud ice water path water vapor profiles
AMPR	10.7, 19.35, 37.1 85.5 Ghz	cross track	40 km	0.65-2.8 km	surface emissivities cloud liquid water path, rainfall sea ice concentration, age
CLS	1064, 532 nm	nadir			cloud boundaries vertical structure (thin clouds)
HIS	3-17 μm 0.5 cm^{-1} resolution	nadir		2 km	surface temperature profiles of T, H ₂ O(g), O ₃ cloud height, emissivity particle size and phase
SSFR	300-2200 μm 5-15 nm resolution	zenith, nadir			reflectance and transmissivity surface spectral albedo cloud phase, optical depth
AirMISR	433, 555, 670, 865 nm	9 look angles			cloud top geometry
C-130					
RAMS	solar, IR	zenith, nadir		hemispheric	solar and IR fluxes albedo, optical depth
AIMR	37, 90 Ghz		13 km	70-180 m	cloud liquid water path, rainfall sea ice concentration, age
MCR	0.63, 0.761, 0.763 1.06, 1.64, 2.16, 10.8 μm	cross track	8 km	28 m	cloud fraction and optical depth particle size and phase
UWa Convair 580					
CAR	13 wavelengths 470-2300 nm	scanning			absorption, scattering of SW bidirectional reflectance function
SSFR	300-2200 nm 5-15 nm resolution	zenith, nadir			bidirectional reflectance and transmissivity surface spectral albedo cloud phase, optical depth
Canadian Convair 580					
lidar	1.064 μm polarization	nadir, zenith			backscatter, depolarization ratio cloud height, particle shape
Landsat Simulator	504-597, 598-700, 702-798, 805-1042 nm	scanning			

Table 3. Cloud microphysical and aerosol instruments on the medium-altitude aircraft: NCAR C-130 (C-130), University of Washington Convair 580 (UWa), and Canadian Convair 580 (CAN).

Instrument	Parameter	Range	C-130	UWa	CAN
Passive Cavity Aerosol Spectrometer Probe PCASP-100	aerosol size distribution	0.1-3.0 μm (diameter)	x	x	x
Condensation Nuclei Particle Counter	total aerosol concentration		x	x	x
Forward Scattering Spectrometer Probe FSSP-300	size and concen of aerosol and drops	0.3-20 μm (diameter)	x	x	x
FSSP-100	cloud drop size dist. and concentration	2-47 μm (diameter)	x	x	x
Scanning Humidigraph	effect of RH on aerosol light scattering	30%<RH<85%		x	
Laser Aerosol Spectrometer-200	aerosol size dist.	0.5-11 μm		x	
Differential Mobility Particle Spectrometer	aerosol size dist.	0.01-0.6 μm		x	
1-D Optical Array Probe (OAP) 260X Cloud Probe	drop and crystal size distribution	40-600 μm (length)	x	x	x
2-D OAP Cloud Probe	drop and crystal shape and size dist.	25-800 μm (length)	x	x	x
2-D OAP Precipitation Probe	rain and snow particle shape and size dist	200-600 mm (length)	x		x
2-D OAP Grey probe	particle shape and size dist	25-1600 μm			x
SPEC Cloud Particle Imager (CPI)	digital images of cloud particles	5-2300 μm	x	x	x
Cloudscope	mass and size dist. of ice particles		x		x
DRJ replicator	images of cloud particles				x
King Hot-wire Probe	liquid water content	0.05-3 g m^{-3}	x		x
Johnson-Williams Probe	liquid water content	0-2 g m^{-3}	x		
Gerber PVM-100A	liquid water content drop effective radius	0.05-3 g m^{-3}	x	x	
Icing Detector	supercooled liquid water content	0.001 - 1 g m^{-3}	x		x
Nevzerov Probes	liquid water content				x
Counterflow Virtual Impactor (CVI)	condensed water content in-cloud aerosol char	impacts cloud part d = 5 - 30 μm			x
Cloud Condensation Nucleus Spectrometer	CCN spectra	supersaturation range 0.01-2%	x		x
Continuous Flow Diffusion Chamber (CFD)	concentration and composition of IFN		x		

Table 4. Distribution of cases for medium-altitude aircraft: NCAR C-130 (NCAR), UWa Convair 580 (UWa), and Canadian NRC Convair 580 (CAN).

	Number of Cases			
	NCAR	UWa	CAN	TOTAL
<i>Cloud Conditions</i>				
Clear	2	1		2
Open leads	0	0	8	8
Cloudy Boundary Layers				
Liquid	4	10	3	17
Ice			1	1
Mixed Phase	3	7	6	16
Cirrus and Altostratus	6	4	9	15
Storm (precipitation)	2	1		3
<i>Flight Patterns</i>				
Mapping of surface features	15			15
Surface albedo and radiation fluxes	14	8		22
Validation of surface remote sensing instruments	13	14	6	33
Cloud radiative properties	14	8	4	28
Cloudy boundary layer	7		8	15
Bidirectional reflectance		15		15

Table 5. Comparison of observations (OBS) with model output (ECMWF, ARCSyM, CSU) for a single grid cell centered at the SHEBA ship for the month of May, 1998.

PARAMETER	OBS	ECMWF	ARCSyM	CSU
downwelling longwave radiation ($W m^{-2}$)	234	222	218	191
downwelling shortwave radiation ($W m^{-2}$)	56	113	77	105
total cloud fraction	0.82	0.69	0.71	0.89
liquid water path ($g m^{-2}$)	38	5	4	12
cloud top height (top layer) (km)	3.3	3.2	5.3	6.9
cloud base height (bottom layer) (km)	1.2	1.0	1.5	1.9

FIGURES

Figure 1: Map showing drift of the SHEBA ship.

Figure 2: Time series of a) cloud radar and b) lidar depolarization observations from the SHEBA ship for 4 May, 1998. In a), the lidar reflectivity shows a boundary layer cloud at altitudes below about 1 km with reflectivity of about -10 dBz, and an altostratus cloud (about -40 dBz) at higher levels that is gradually diminishing with time. In b), the lidar is attenuated by liquid water at altitudes above about 800 m, with depolarization ratios less than 0.2 indicated the presence of liquid water.

Figure 3: Vertical profile of cloudy boundary layer on 4 May, 1998 at 2300 UTC from the NCAR C-130Q. a) Temperature, b) water vapor mixing ratio; c) liquid water content (solid) determined by the King Probe and ice water content (dash) determined by the Cloud Particle Imager (CPI).

Figure 4: Observations of cloud particles from the Cloud Particle Imager (CPI) obtained from the C-130Q on 4 May, 1998. Profile segment heights, average temperatures and average particle concentrations are listed at the left for above cloud top, just below cloud top, in middle of cloud, and in the precipitation region. Representative images of ice particles (middle left) and water drops (right) are shown for each profile segment. Size distributions for ice particles (middle right) and water drops (right) are averaged over time period for each profile segment.

Figure 5: Data obtained from a transect flown at 300 m altitude by the Canadian Convair 580 aircraft across Cape Bathurst Polynya in the Beaufort Sea ($70^{\circ}12'N$, $134^{\circ}45'W$) on April 25, 1998. The polynya is shown in d) between points A and B. a) air temperature (thin) and its vertical turbulent flux (bold); b) specific humidity (thin) and its vertical turbulent flux (bold); c) reflected solar radiation flux in the wavelength interval 0.45-0.52 μm .

Figure 6. Observations from the downward looking lidar obtained by the Canadian Convair-580 on 27 April, 1998 across the Cape Bathurst Polynya in the Beaufort Sea (near 70°N, 134.5°W). The upwind edge of the polynya is near the left edge of the figure. The scale bar represents backscatter ratio (no units), from 0 to 10, indicating the amount of scatter relative to "clear" air. The cloud plume is shown by the highest backscatter values. The growth of the internal boundary layer over the polynya is indicated by the solid line.

Figure 7: Vertical profiles of the aerosol light-scattering coefficient, σ_{scat} (dotted line) and the aerosol light-extinction coefficient, σ_{ext} (solid line) at a relative humidity of 30% and a wavelength of 550 nm. The measurements were obtained aboard the University of Washington's Convair-580 aircraft over the Barrow ARM site between 224700 and 244200 UTC on 19 June 1998.

Figure 8. Time series plot from 4 May through 24 June 1998 of average surface albedos obtained from the C-130Q (May, July) and the UWa Convair-580 (June) in the vicinity of the SHEBA ship. Broadband surface albedo measurements (300-3000 nm) in the vicinity of the SHEBA ship.

Figure 9: Time series plot of upwelling longwave (red) and shortwave (blue) radiation obtained by the NCAR C-130 at an altitude of 30 m for 7 May 1998. The location of leads is indicated in green.

Figure 10 Observations of spectral downwelling solar irradiance obtained from the Solar Spectral Flux Radiometer at the SHEBA ship on 15-16 May, 1998.

Figure 11 Bidirectional reflectance function obtained from the Cloud Absorption Radiometer (CAR) on the UWa Convair-580 .at 0.68 and 1.64 μm for a) the sea ice surface on June 23, 1998 at 77°44' N, 16°36' W when the solar zenith angle was 54.45°; and b) homogeneous stratus cloud on 29 May, 1998 at 72°48' N, 158°44' W when the solar zenith angle was 53.65°.

Figure 12 Composite of observations obtained from the NASA ER-2 aircraft on 20 May, 1998 in the vicinity of the coast off Barrow. MAS: MODIS Airborne Simulator; AMPR: Advanced Microwave Precipitation Radiometer; MIR: Millimeter-wave Imaging Radiometer; CLS: Cloud Lidar System.

Fig. 13. NOAA-14 AVHRR image and derived cloud radiation products over SHEBA (denoted as "S" in each panel) and the surrounding ice pack at 2252 UTC 4 May 1998. a) visible, 1-km resolution image with box outlining area of cloud analysis; b) cloud mask with coincident C-130Q flight track; c) broadband shortwave albedo; d) outgoing longwave radiation in Wm^{-2} ; e) 3.7- μm image (left panel) and derived effective cloud particle sizes, in μm , r_e refers to effective radius of liquid water droplets, D_e denotes effective diameter of ice cloud particles; and gray areas indicate that no size could be retrieved.

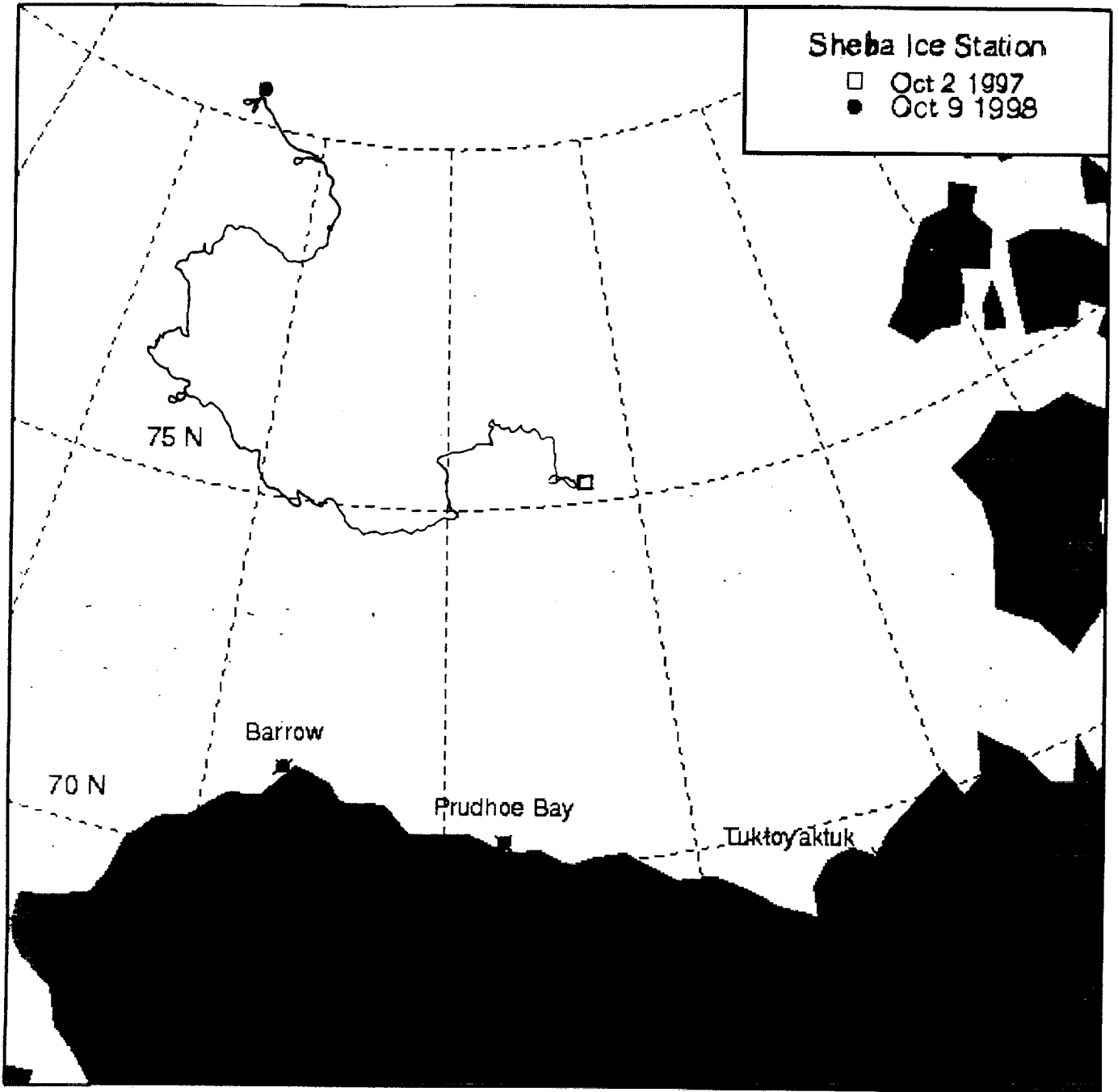
Fig. 14. NOAA-15 AVHRR 1-km imagery at 2021 UTC 26 July 1998 over the Arctic Ocean. The location of the SHEBA ship is denoted with an "S." a) 0.63- μm image; b) 11- μm image; c) 1.6- μm image; and d) pseudo-color image with red, green, and blue intensities determined by the 0.63- μm reflectance, 1.6- μm reflectance, and the reversed 11- μm temperature (snow: pink, open water: dark blue, thick water cloud: white, ice clouds: light blue-gray).

Figure 12 Composite of observations obtained from the NASA ER-2 aircraft on 20 May, 1998 in the vicinity of the coast off Barrow. MAS: MODIS Airborne Simulator; AMPR: Advanced Microwave Precipitation Radiometer; MIR: Millimeter-wave Imaging Radiometer; CLS: Cloud Lidar System.

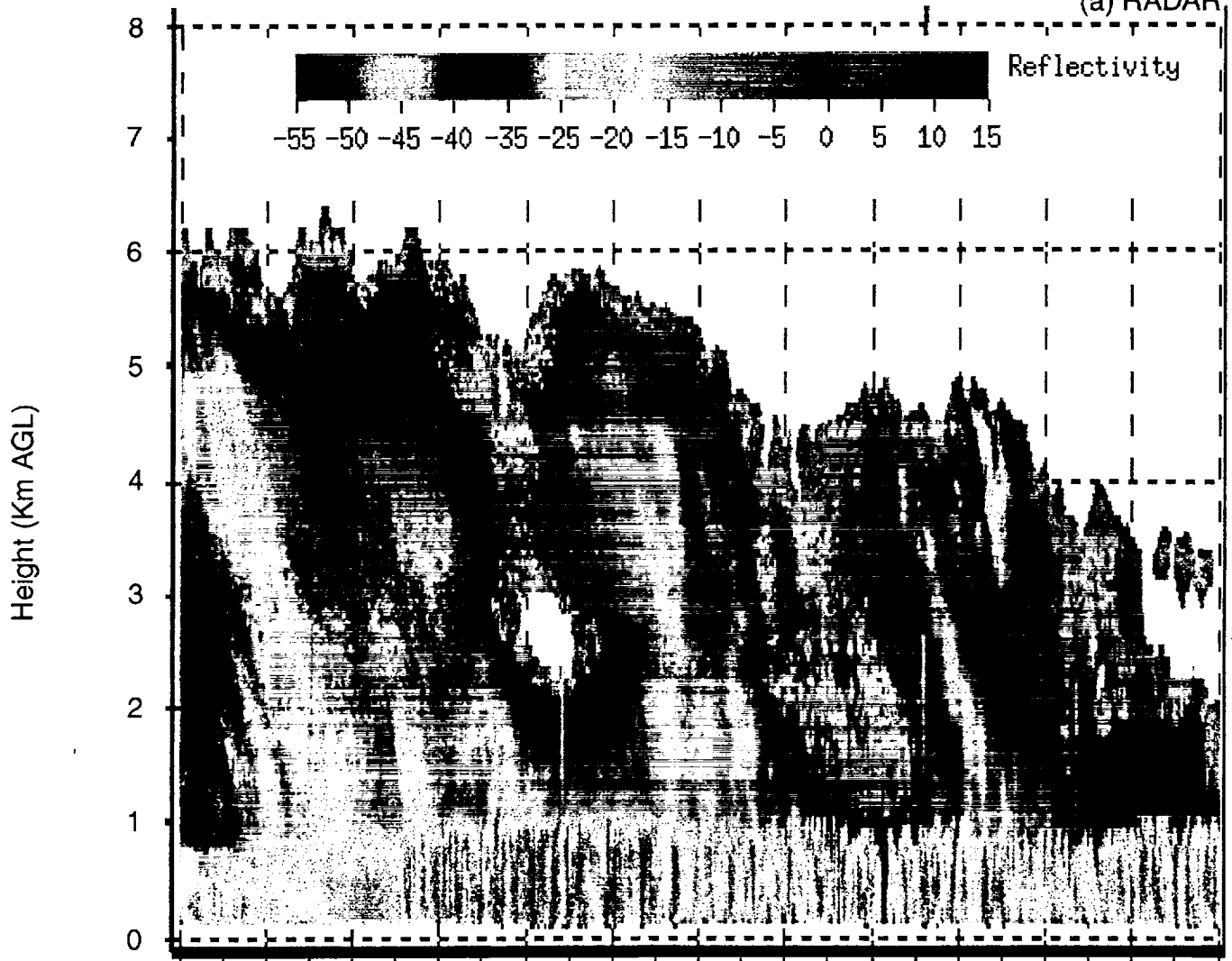
Fig. 13. NOAA-14 AVHRR image and derived cloud radiation products over SHEBA (denoted as "S" in each panel) and the surrounding ice pack at 2252 UTC 4 May 1998. a) visible, 1-km resolution image with box outlining area of cloud analysis; b) cloud mask with coincident C-130Q flight track; c) broadband shortwave albedo; d) outgoing longwave radiation in Wm^{-2} ; e) 3.7- μm image (left panel) and derived effective cloud particle sizes, in μm , r_e refers to effective radius of liquid water droplets, D_e denotes effective diameter of ice cloud particles; and gray areas indicate that no size could be retrieved.

Fig. 14. NOAA-15 AVHRR 1-km imagery at 2021 UTC 26 July 1998 over the Arctic Ocean. The location of the SHEBA ship is denoted with an "S." a) 0.63- μm image; b) 11- μm image; c) 1.6- μm image; and d) pseudo-color image with red, green, and blue intensities determined by the 0.63- μm reflectance, 1.6- μm reflectance, and the reversed 11- μm temperature (snow: pink, open water: dark blue, thick water cloud: white, ice clouds: light blue-gray).

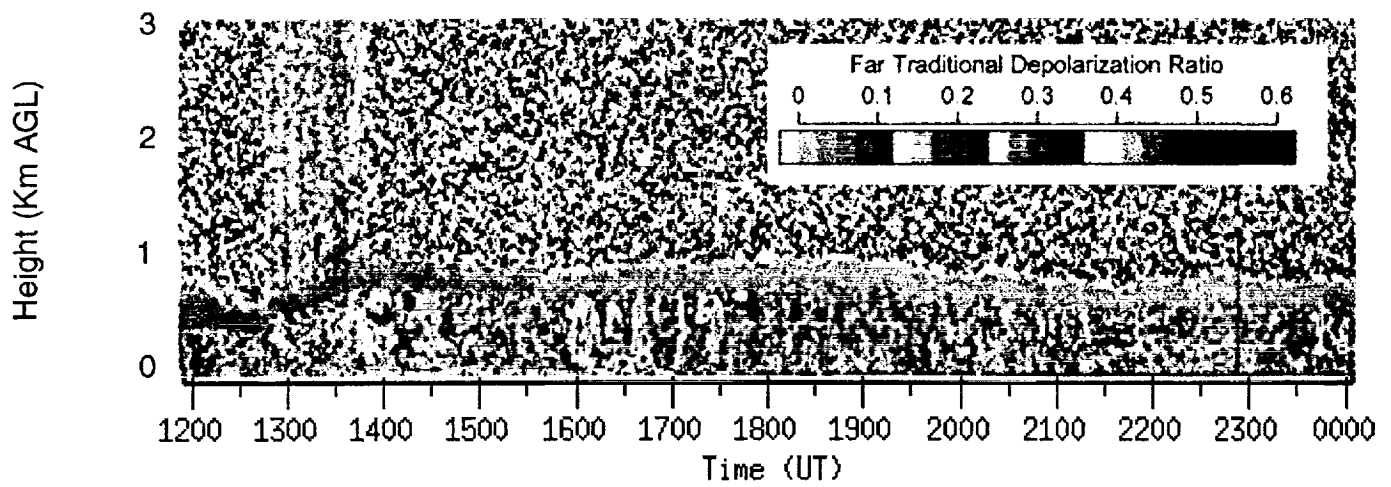
Fig. 15. Comparison of simulations of the ARCSyM and CSU single-column models with SHEBA observations during the month of May. a) liquid water path; b) downwelling surface longwave radiation; c) net surface shortwave radiation.

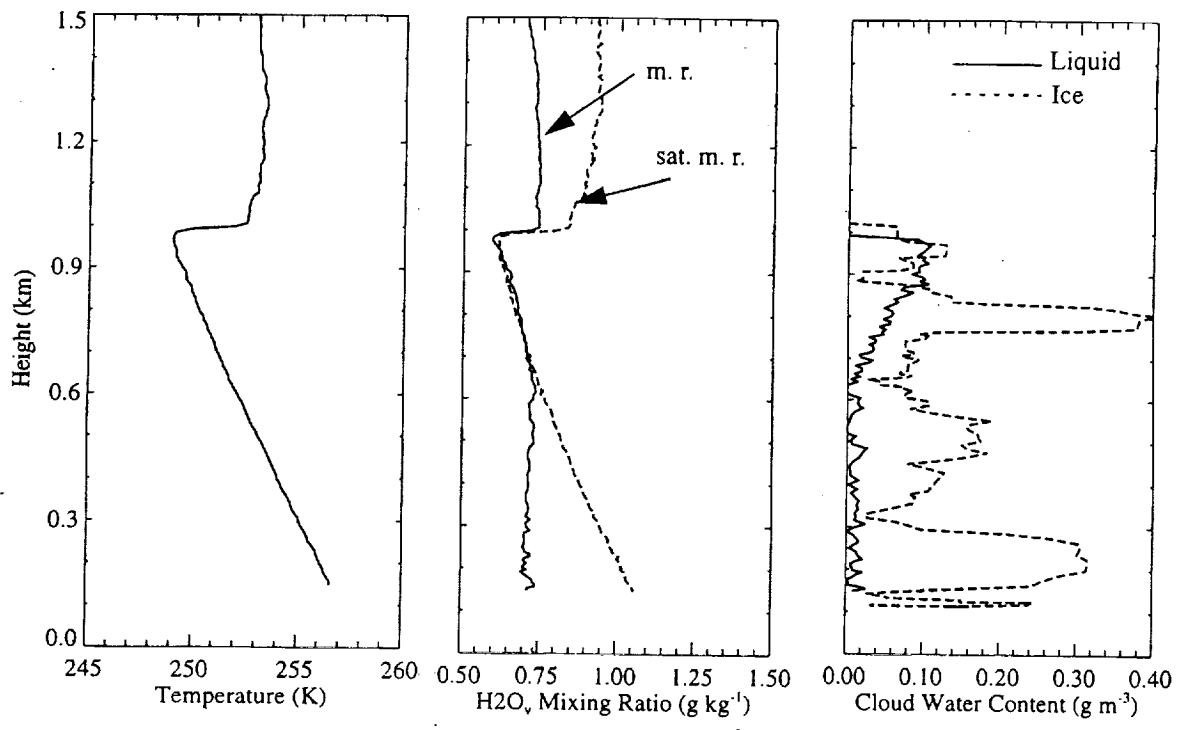


(a) RADAR

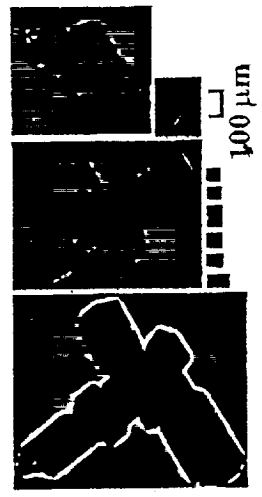


(b) LIDAR

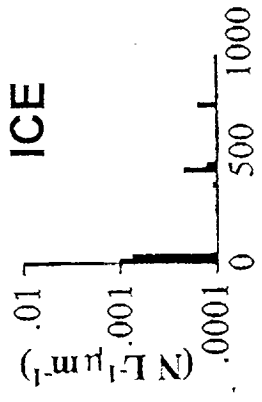




ABOVE
1060 m
-21.0 C
10 L⁻¹



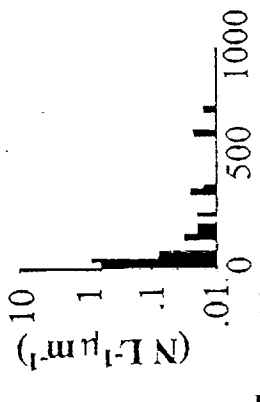
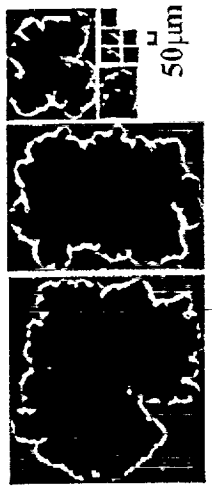
ICE



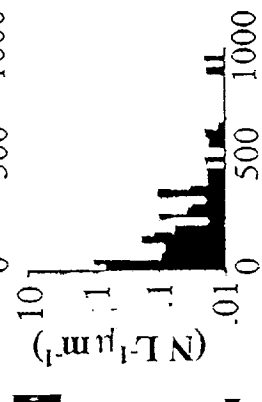
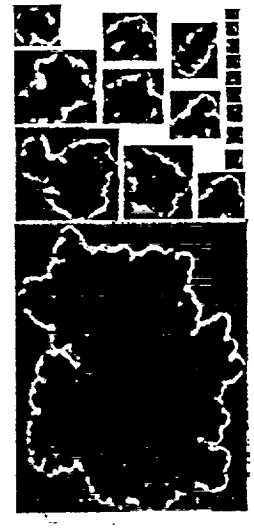
LIQUID



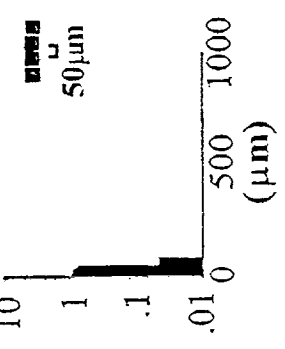
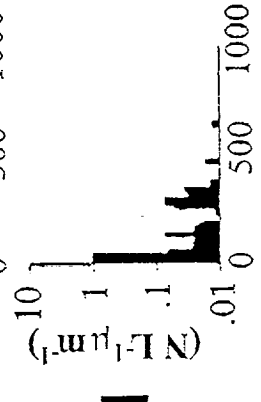
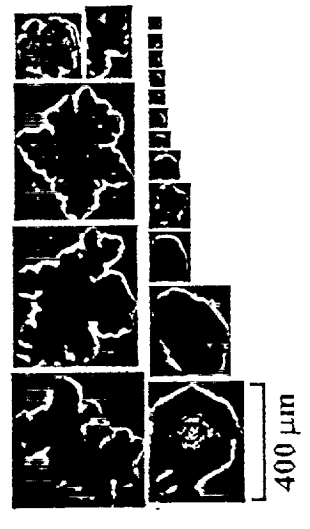
TOP
900-1050 m
-23.5 C
350 L⁻¹

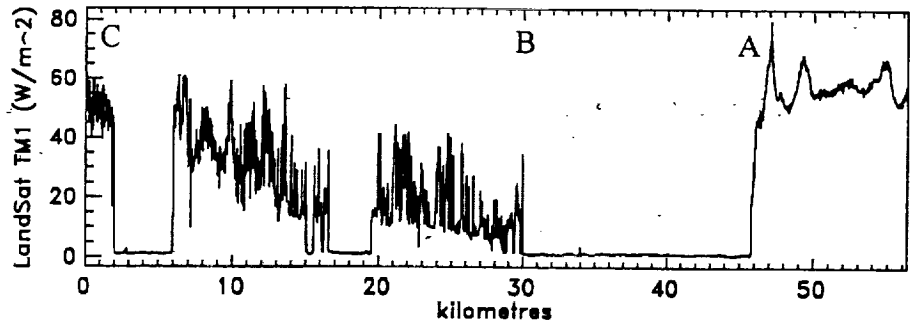
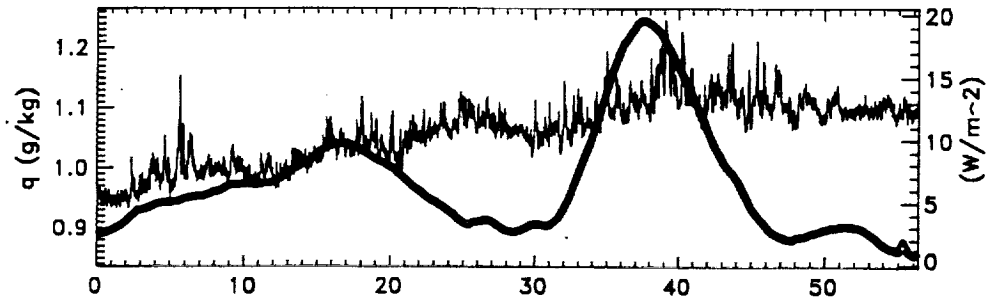
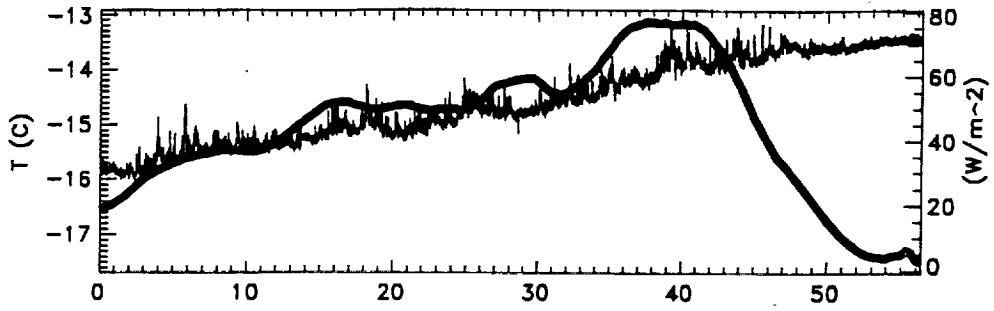


MIDDLE
750-900 m
-23.5 C
200 L⁻¹

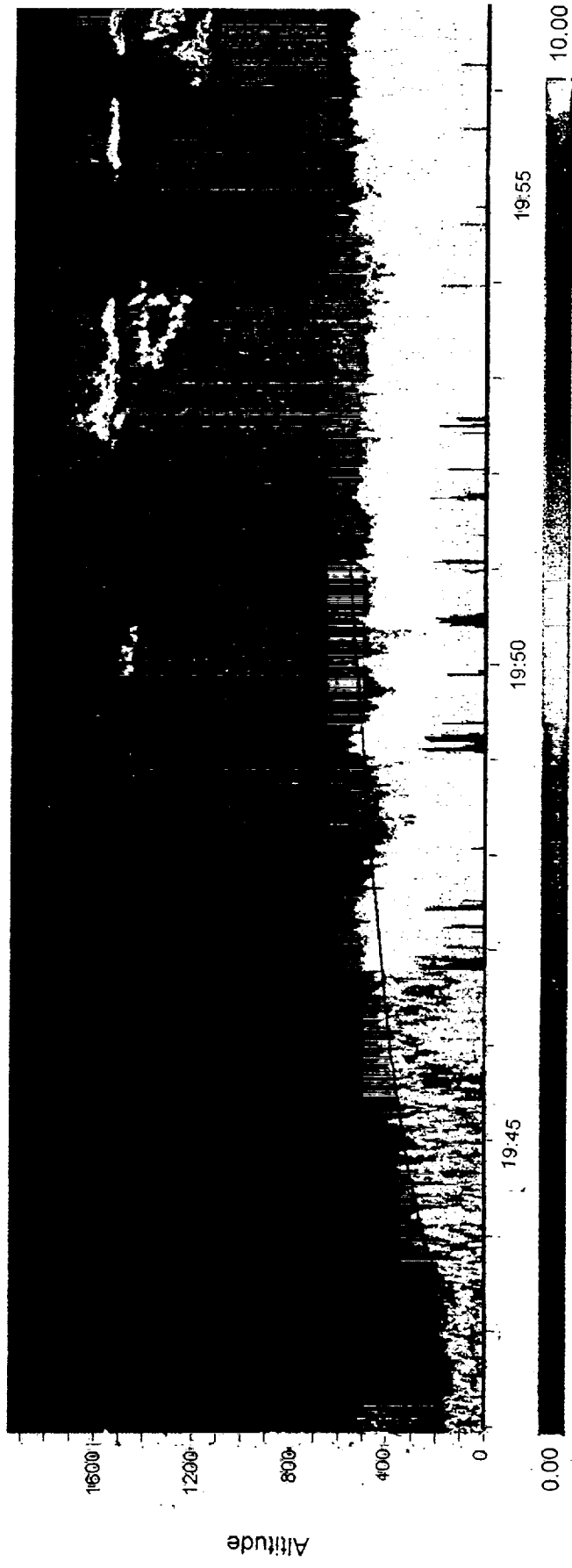


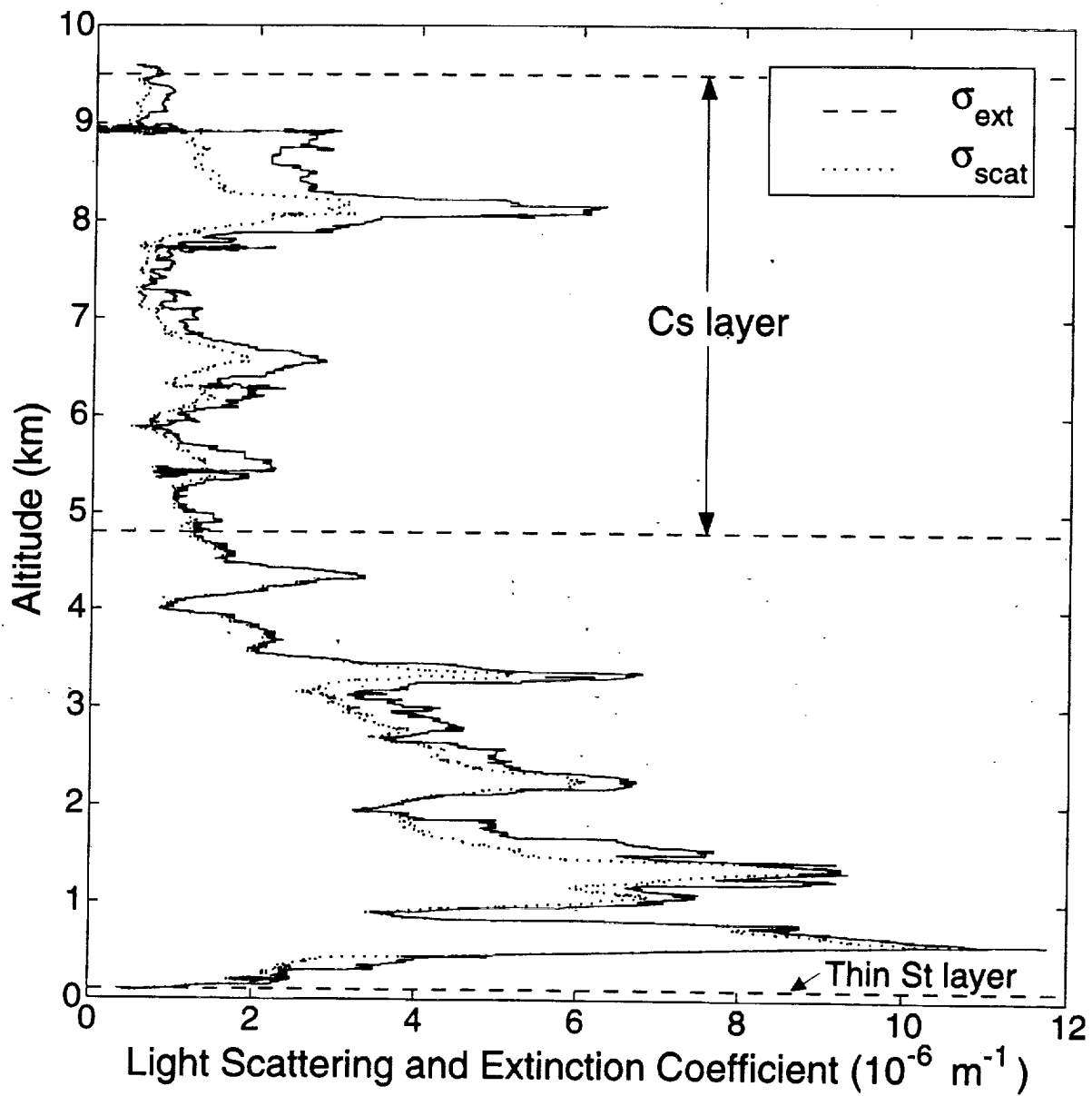
PRECIP
100-750 m
-21.0 C
150 L⁻¹

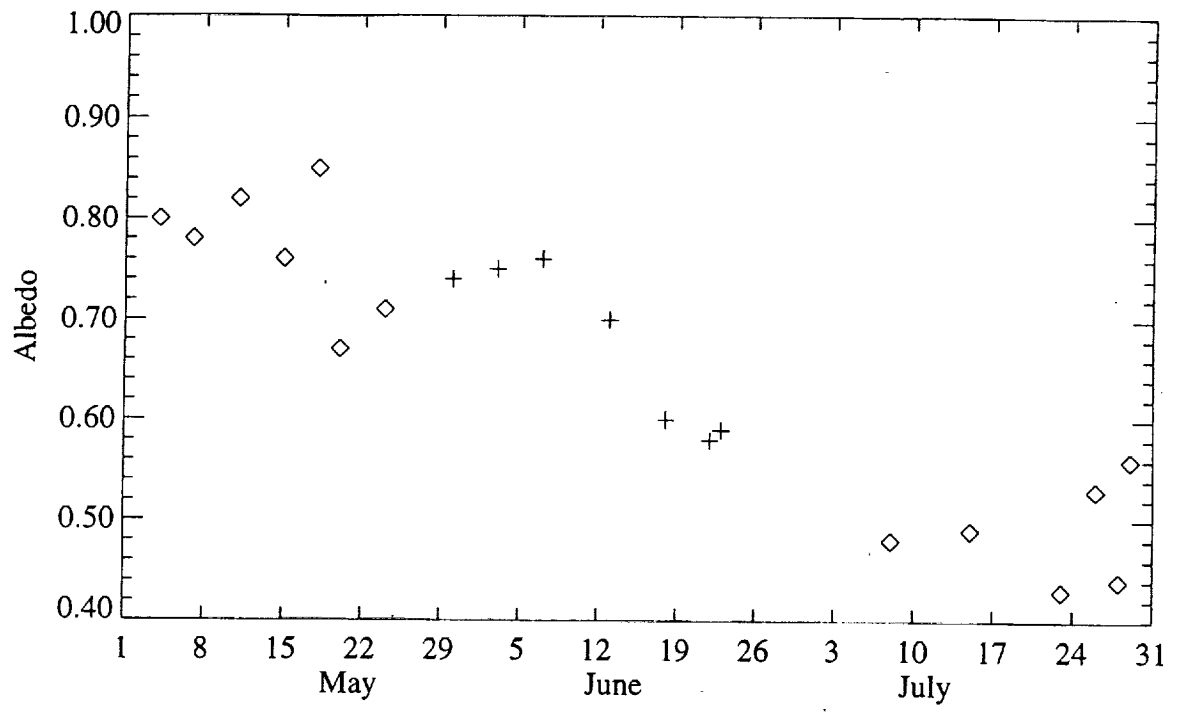


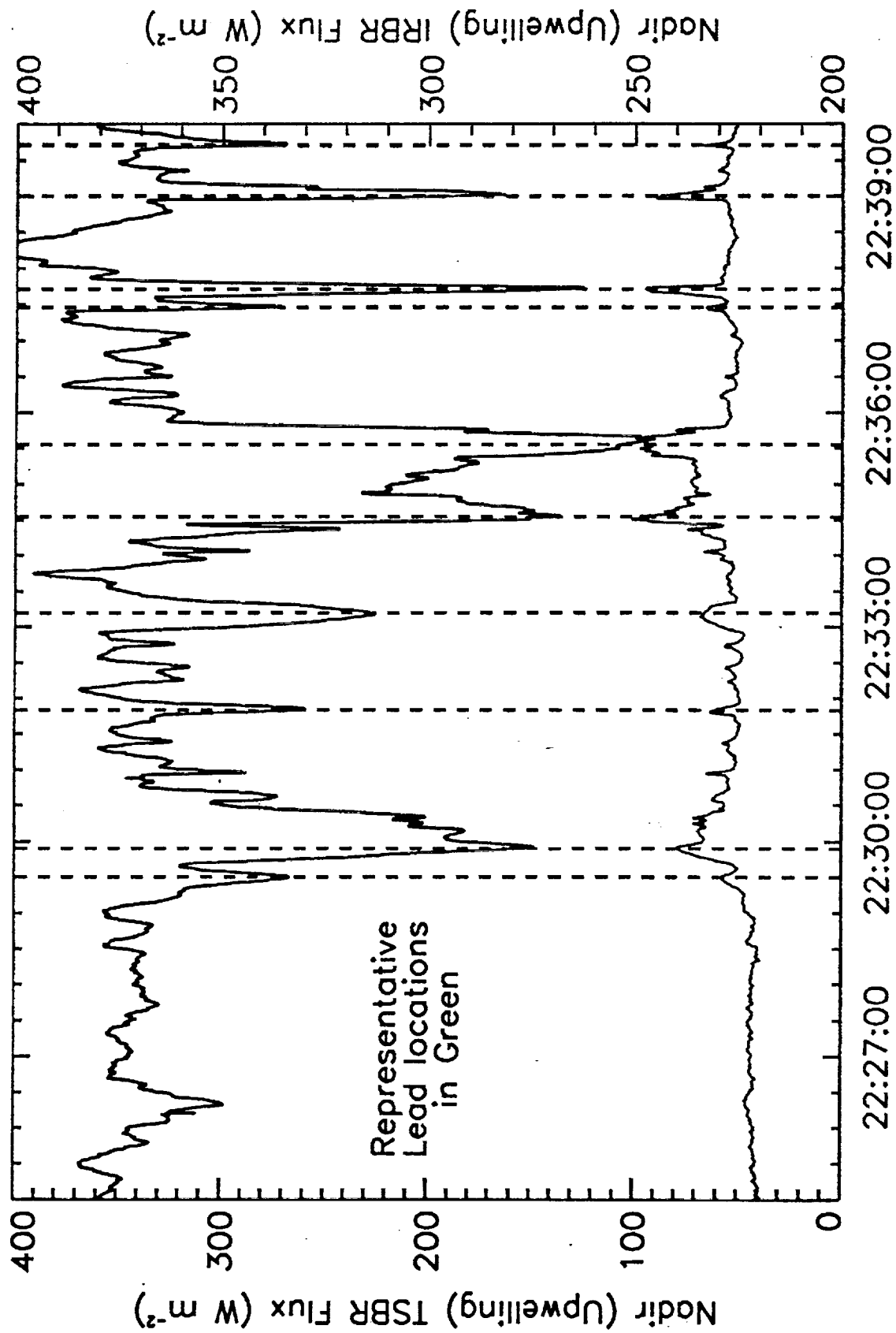


9





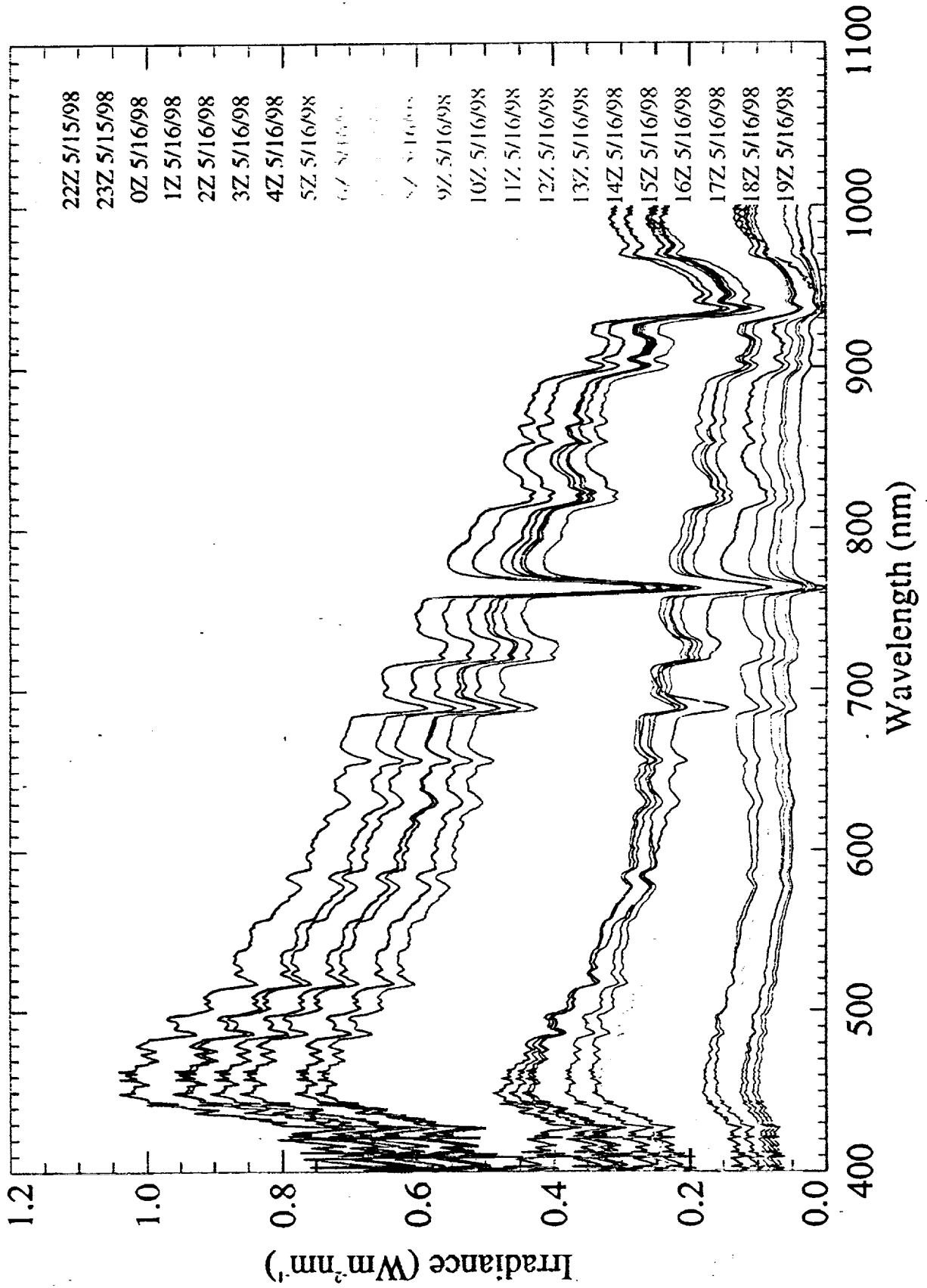


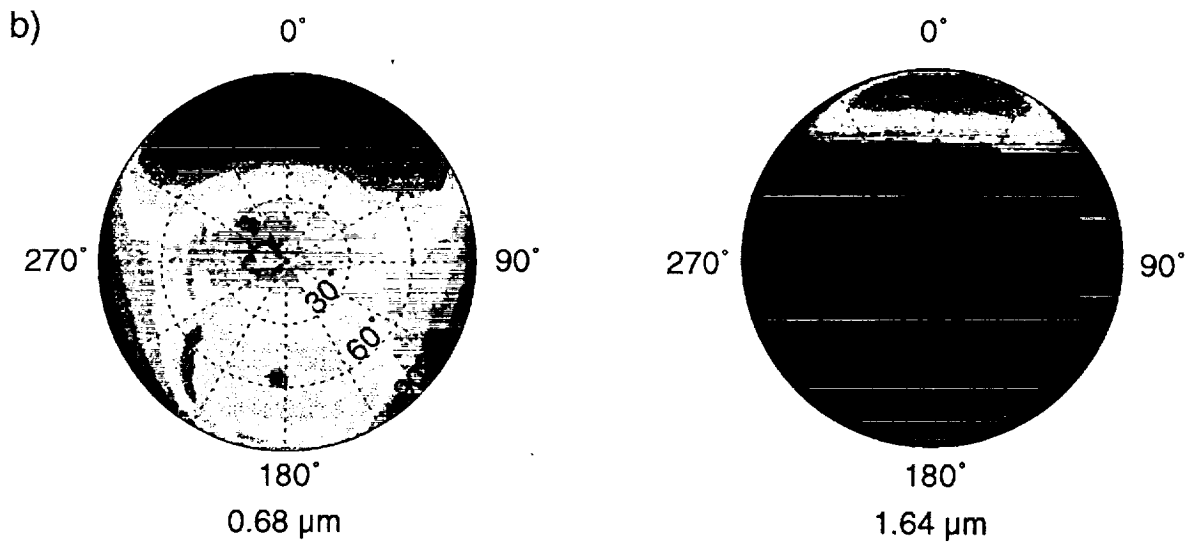
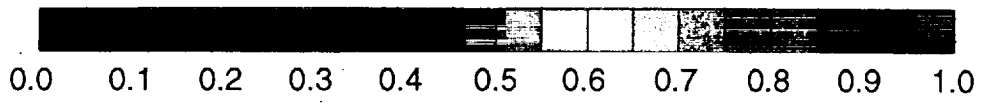
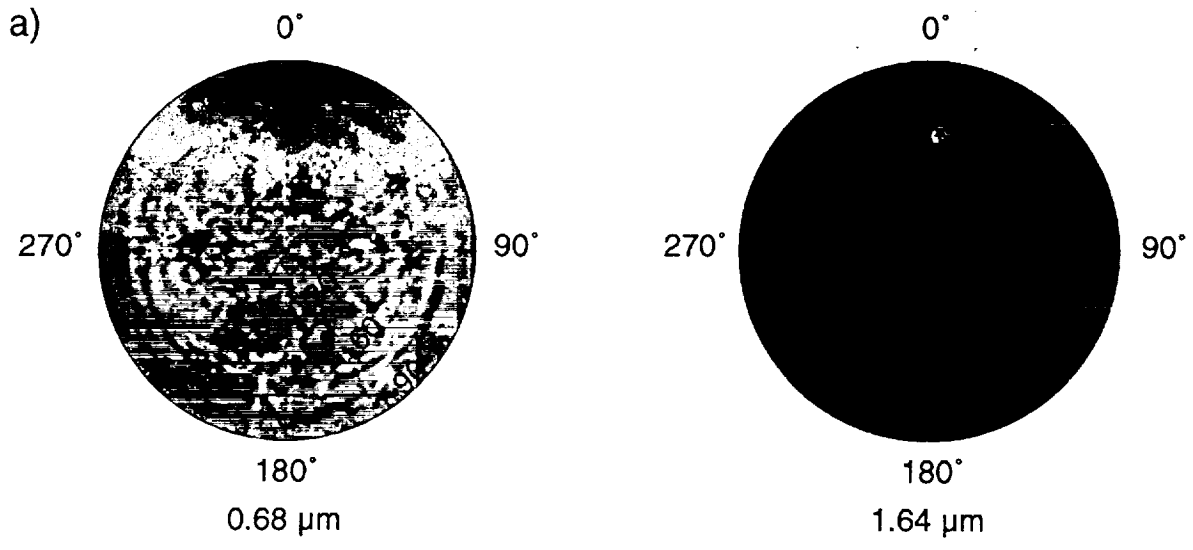


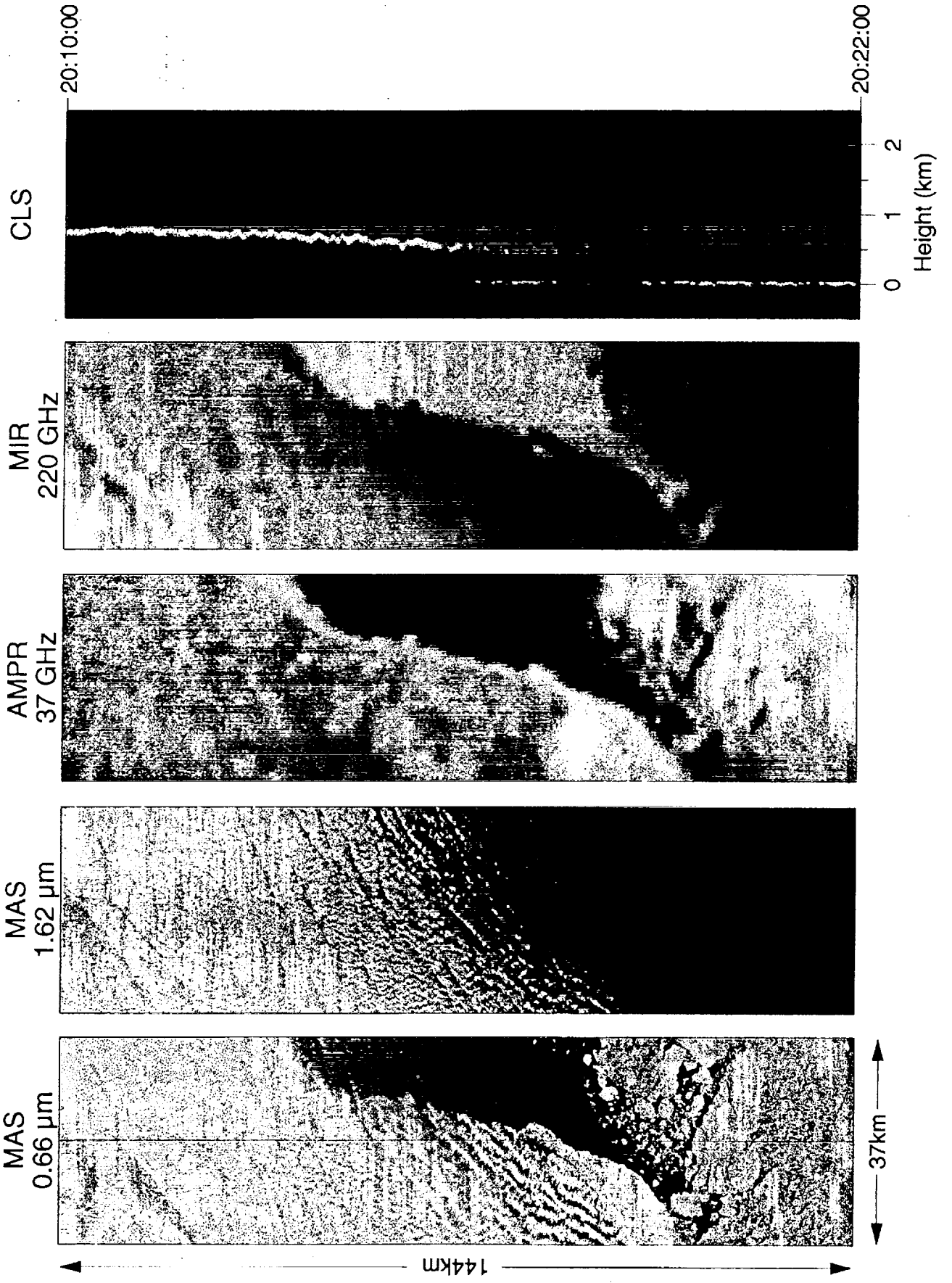
Representative
Lead locations
in Green

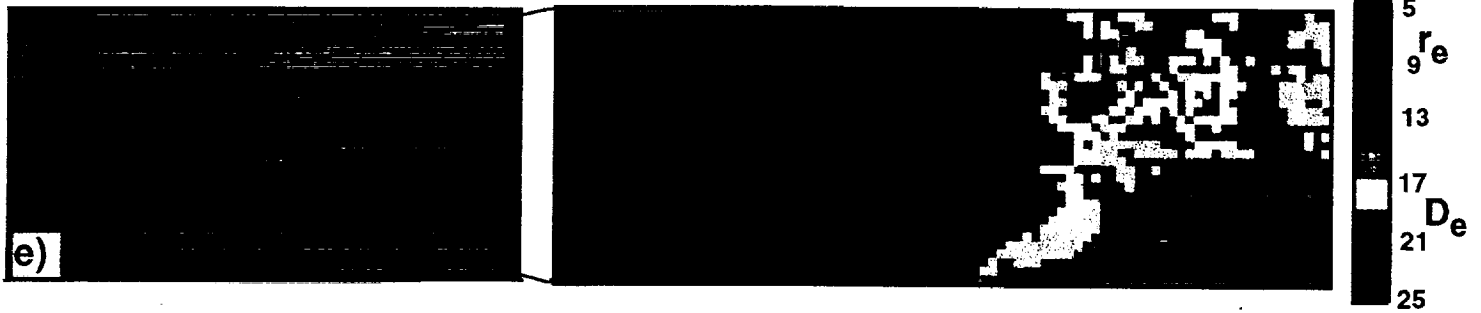
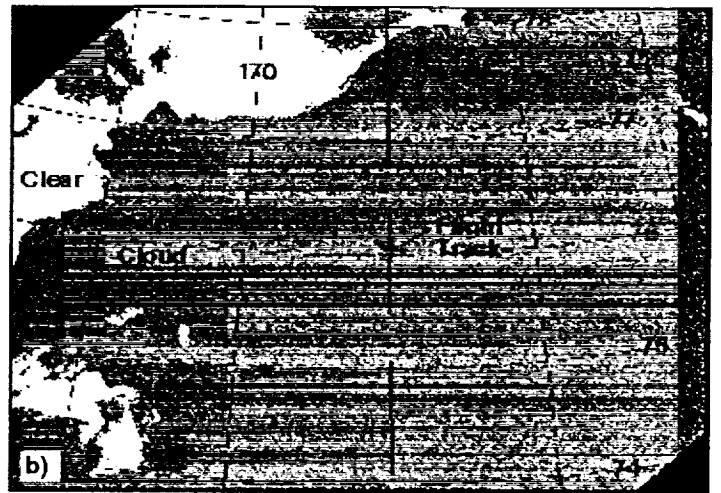
Nodir (Upwelling) TSBR Flux ($W m^{-2}$)

Nodir (Upwelling) IRBR Flux ($W m^{-2}$)









5.9.1

